Unravelling the architecture and evolution of the inverted multi-stage North Iberian-Bay of Biscay rift

Patricia Cadenas, Gianreto Manatschal, Gabriela Fernández-Viejo

Unravelling the architecture and evolution of the inverted multi-stage North Iberian-Bay of Biscay rift

Patricia Cadenas, Gianreto Manatschal, Gabriela Fernández-Viejo

PII: S1342-937X(20)30221-5

DOI: https://doi.org/10.1016/j.gr.2020.06.026

Reference: GR 2396

To appear in: *Gondwana Research*

Received date: 11 January 2020

Revised date: 29 June 2020

Accepted date: 29 June 2020

Please cite this article as: P. Cadenas, G. Manatschal and G. Fernández-Viejo, Unravelling the architecture and evolution of the inverted multi-stage North Iberian-Bay of Biscay rift, *Gondwana Research* (2020), https://doi.org/10.1016/j.gr.2020.06.026

Unravelling the architecture and evolution of the inverted multi-stage North Iberian-Bay of Biscay rift

Patricia Cadenas[a*], Gianreto Manatschal[a], Gabriela Fernández-Viejo[b]

(a): Institut du Physique du Globe de Strasbourg, UMR 7516, CNRS, University of Strasbourg/EOST, 1, rue Blessig, 67000, Strasbourg, France. patri.geo.moal@gmail.com ; manat@unistra.fr

(b): Department of Geology, University of Oviedo, C/Jesús Arias de Velasco, s/n, 33005, Oviedo, Asturias, Spain. fernandezgabriela@uniovi.es

***corresponding author:** patri.geo.moal@gmail.com

Abstract

Current rift models propose polyphase rift evolutions that develop with the same kinematic framework and accommodate continuous and sequential extension, through the stacking of deformation modes. Several rifted margins show, however, evidence for multiple and out of sequence rift events, which developed within different kinematic frameworks, with a complex spatial and temporal evolution. In this work, we address the problem of multi-stage rift systems based on the study of the central North Iberian margin, located at the southern Bay of Biscay triangular oceanic domain. This magma-poor rifted margin recorded three major Mesozoic rift events and a subsequent Alpine compressional reactivation, representing a unique setting to study the architecture of a multi-stage rift system and the exerted control on subsequent reactivation. Relying on a dense set of 2D seismic reflection profiles, boreholes, and published velocity models, we map and describe structural domains and major extensional and compressional structures, and we construct depth and thickness maps of syn-rift units. These new maps display the geometry and spatial distribution of major rift basins and bounding structures. Distinctive scenarios resulting from this tectono-stratigraphic approach led us to define three rift systems. A first, diffuse and widespread Triassic system, with classical fault-bounded half-graben basins; a second, narrow, deep and localised Late Jurassic to

Barremian transtensional system, including laterally confined pull-apart basins; and a third, widely distributed Aptian to Cenomanian hyperextended system. Our results show that each rift system controlled the successive extensional and compressional events, resulting in a complex 3D template. Deciphering the tectono-stratigraphic architecture of such, multi-stage systems provide key insights on the spatial, temporal, and thermal evolution of divergent plate boundaries. It is likewise indispensable to propose and test kinematic plate deformable models on conjugate rifted margins and to comprehend the implications for their reactivation.

Keywords: multi-stage extension, rift system, strike-slip, hyperextension, compressional reactivation, 3D structural segmentation.

1) Introduction

Extensional models describing the evolution of rifting and the architecture of passive margins have evolved remarkably over the past years. The pure-shear (*McKenzie*, 1978) and simple-shear (*Wernicke*, 1985) classical end member models considered rifting as a mono-phase event. During the last two decades, extensive research, including seismic and drilling surveys at present-day margins, studies of fossil remnants preserved in orogens, and dynamic modelling, led to the conclusion that rifting is rather a poly-phase and strain localisation process, which implies the stacking of successive rift phases, governed by particular modes of deformation (e.g, *Lavier and Manatschal*, 2006*; Péron-Pinvidic and Manatschal*, 2009). Poly-phase models have assumed that these phases develop in sequence during a unique rift event within the same kinematic framework, leading to the migration of extension toward the locus of future breakup (e.g., *Bertotti et al.*, 1993; *Santantonio & Carminati*, 2011; *Péron-Pinvidic et al.*, 2013). Poly-phase rift systems have been described from the southern Atlantic (e.g., *Zalan et al.*, 2011; *Norton et al.*, 2016), and the North Atlantic (e.g., *Reemst and Cloetingh*, 2000; *Pereira and Alves*, 2012; *Bell et al.*, 2014). In the

southern North Atlantic, however, sequences of distinct rifting events have been recognized (e.g., *Alves et al.*, 2009; *Gouiza et al.*, 2017). The kinematics and the temporal evolution of each rift event and the spatial imprint of the resulting multi-stage systems remain at present poorly understood.

In magma-poor rifted margins, the migration and stacking of deformation modes during continuous extension, from stretching, thinning and exhumation, to the onset of oceanic accretion, results in major crustal thinning and related accommodation space (e.g., *Lavier and Manatschal*, 2006; *Perón-Pinvidic and Manatschal*, 2009). Polyphase fault systems control crustal attenuation and the development of rift-related basins (*Reston*, 2005; *Ranero and Pérez-Gussinyé*, 2010; *Péron-Pinvidic et al*., 2013; *Sutra et al.*, 2013; *Lymer et al.*, 2019; *Phillips et al.*, 2019). The distribution, thickness, and geometry of the sedimentary infill, the nature and thickness of the crust, and the fault architectures, are the typical features defining the architecture of magma-poor rifted margins (e.g., *Péron-Pinvidic et al.*, 2013; *Tugend et al.*, 2014). To capture all these features, new methodological approaches, which have been referred to as "rift domains mapping", developed (*Tugend et al.*, 2015). Nevertheless, the use of this approach remains challenging in multi-stage rift systems, mainly because these systems can result from the stacking of different out of sequence rift events developed in different kinematic frameworks. Deciphering the architecture of such systems asks therefore for a detailed tectono-stratigraphic characterization of each rift system in order to figure out their spatial overprint.

In this study, we focus on the central part of the magma-poor and multi-stage North Iberian margin, which includes the Asturian Basin, the Le Danois High and the Biscay abyssal plain as major physiographic features (figure 1a). The aim is to identify and define rift systems resulting from distinctive rift events, to describe their architecture, and to map their bounding structures and spatial distribution. This approach enables the characterization of the multi-stage rift system and to better constrain the related rifting processes and the unequal development of rift basins along the Iberian/European plate boundary during the Mesozoic. It also adds up new outcomes to test the

various and strongly debated kinematic scenarios of the Iberian plate during this period (e.g., *Barnett-Moore et al.,* 2016 and references therein) and to understand the subsequent margin reactivation during the Alpine convergence.

2) Tectonic Setting

The Bay of Biscay corresponds to a v-shaped oceanic basin that developed along the Iberian/European plate boundary, together with the Pyrenean and Basque Cantabrian rift systems (e.g., *Vergés and García-Senz*, 2001; *Tugend et al.*, 2014; *Tavani et al.*, 2018) (figure 1b). It represents a failed arm of the southern North Atlantic, which opened during the Mesozoic and was subsequently partially closed from Late Cretaceous to Cenozoic during the Alpine Orogeny (e.g, *Srivastava et al.*, 2000; *Thinon et al.*, 2003; *Sibuet et al.*, 2004; *Vissers and Meijer*, 2012). Its opening and partial closure in the context of the Iberian plate kinematics is still a matter of debate. The proposed models include a scissor-type opening, a strike slip displacement, and a mixed model consisting of transtensional and orthogonal deformation (see *Barnett-Moore et al.*, 2016 and references therein). The North Iberian margin corresponds to the southern margin of the Bay of Biscay (figure 1a). Early stages of extension have been ascribed to an undifferentiated Permo-Triassic post-Variscan event (e.g., *Rat*, 1988; *García-Mondéjar*, 1996; *Ziegler and Dezès*, 2006), and to a shorter Middle to Late Triassic event, which led to the development of half-grabens (e.g., *Zamora et al*., 2017; *López-Gómez et al.*, 2019). A major extensional event spanned from Late Jurassic to Barremian (e.g., *Montadert et al*., 1971; *Boillot et al.*, 1979; *Déregnaucourt and Boillot*, 1982; *García-Mondéjar*, 1996; *Thinon et al.*, 2002; *Ferrer et al*., 2008; *Jammes et al*., 2009; *Tugend et al.*, 2014; *Cadenas et al.*, 2018). Extreme crustal thinning and exhumation at the conjugate North Iberian and Armorican margins preceded seafloor spreading in the western corner of the Bay of Biscay (*Thinon et al.*, 2003; *Jammes et al.*, 2009; *Roca et al*., 2011; *Tugend et al*., 2014; *Cadenas et*

al., 2018). Oceanic accretion occurred during a short-lived late Early to Late Cretaceous event (Latest Aptian to Campanian) (e.g. *Roest and Srivastava*, 1991; *Sibuet and Collette*, 1991; *Sibuet et al.*, 2004). During the Alpine reactivation, incipient subduction and the underthrusting of hyperextended crust and/or exhumed mantle beneath the North Iberian continental platform focused most of the compressional deformation (e.g., *Boillot et al*., 1979; *Déregnaucourt and Boillot*, 1982; *Álvarez-Marrón et al.*, 1997; *Gallastegui et al*., 2002; *Roca et al*., 2011; *Fernández-Viejo et al.*, 2012; *Cadenas et al.*, 2018).

2.1) The central North Iberian margin

The central North Iberian margin is depicted morphologically by a narrow and irregular continental platform and a steep and locally structured continental slope (figure 1a). The Le Danois High and the Santander Promontory represent the most outstanding features (figure 1a). Between 5º30´W and 4º40´W, the Le Danois High separates a narrow rift basin, referred to as the Asturian Basin (*Riaza*, 1996; *Cadenas and Fernández-Viejo*, 2017) or the Le Danois Basin (*Álvarez-Marrón et al.*, 1996; *Roca et al.*, 2011) (figure 1c), from the wide Biscay accretionary wedge (*Álvarez-Marrón et al.*, 1997; *Gallastegui et al.*, 2002; *Fernández-Viejo et al.*, 2011; *Roca et al.*, 2011; *Cadenas et al.*, 2018). Between 3º50´W and 4ºW, the Santander Promontory corresponds to a narrow and prominent N-S structural high, which is bounded by the Santander and Torrelavega canyons (figure 1a). *Roca et al. (2011)* defined this area as a N-S transfer zone, referred to as the Santander Transfer Zone (STZ) (figure 1c). The STZ has been interpreted to accommodate structural variations within the hyperextended rift system and the jump of the Alpine deformation fronts (*Roca et al., 2011*; *Tugend et al*., 2014).

2.1.1) The Asturian Basin

The offshore, WNW-ESE trending Asturian Basin is a slightly reactivated asymmetric rift basin (e.g., *Boillot et al.*, 1979; *Riaza*, 1996; *Gallastegui et al.*, 2002; *Cadenas and Fernández-Viejo*, 2017). Two major bounding faults delimit the main depocentre, which is 13 km thick and overlies a less than 12 km thick continental crust (*Cadenas et al.*, 2018). The sedimentary infill has been divided into six seismo-stratigraphic units (*Cadenas and Fernández-Viejo*, 2017). Considering the rifting processes, these units include three tectonic units: **1)** a pre-kinematic unit, spanning from Lower to Middle Jurassic; **2)** a thick Late Jurassic to Barremian wedge-shaped syn-kinematic unit; and **3)** a post-kinematic unit, including Aptian to Eocene sediments. The mild inversion observed within the Asturian Basin was accommodated through the reactivation of normal faults, resulting in the formation of an Upper Eocene to Lower Miocene fan shaped syn-orogenic unit. These sediments are unconformably overlain by a Middle Miocene to Quaternary post-orogenic unit (*Gallastegui et al.*, 2002; *Cadenas and Fernández-Viejo*, 2017).

2.1.2) The Le Danois High

Along the northern slope of the Le Danois High, samples of granulites were dredged (*Capdevila et al.*, 1980; *Malod et al.*, 1982), with cooling ages ranging from 130 to 52 Ma (*Fügenschuh et al.*, 2003). Two end-member interpretations have been proposed to explain the structure and the evolution of this structural high. *Boillot et al.* (1979), *Malod et al.* (1982), and *Gallastegui et al.* (2002) interpreted the Le Danois High as a stacking of previously extended crust, which developed due to the emplacement of north verging thrusts. *Cadenas et al.* (2018) defined the Le Danois High as a thick crustal block reaching a maximum thickness of about 20 km and interpreted these bathymetric high as a rift-related block that was passively rotated and uplifted during the Alpine compression (figure 1c and d).

2.1.3) The Biscay abyssal plain

The nature of the crust flooring the Biscay abyssal plain in the central North Iberian margin remains unresolved. Using gravity inversion procedures, *Tugend et al.* (2014) interpreted a hyperthinned domain including highly thinned crust less than 10 km thick and an exhumed mantle domain. Based on the interpretation of a dense set of 2D seismic reflection profiles, together with published velocity models, *Cadenas et al.* (2018) interpreted an undifferentiated hyperextended domain including both extremely thinned crust less than 5 km thick and exhumed mantle (figure 1c). Velocities Vp<8 km/s beneath the Moho within the continental slope and platform have been attributed to serpentinized mantle (*Fernández-Viejo et al*., 1998; *Ruiz et al.*, 2017). They may be related to the underthrusting of highly thinned crust and exhumed mantle, which led to the formation of an accretionary wedge at the foot of the slope (*Álvarez-Marron et al.*, 1997; *Gallastegui et al.*, 2002; *Fernández-Viejo et al.*, 2011; *Roca et al.*, 2011; *Fernández-Viejo et al*., 2012; *Cadenas et al*., 2018). The overlying, most likely Aptian to Late Cretaceous sediments, form massive depocentres showing sag-type architectures (*Cadenas et al*., 2018). More than 2 km of Late Cretaceous to Middle Miocene post-tectonic sediments bury this structure (*Álvarez-Marrón et al.*, 1997; *Fernández-Viejo et al.*, 2011; *Roca et al*., 2011, *Fernández-Viejo et al.*, 2012).

3) Data and methods

3.1) Data

We integrated in our study the CS01 dense dataset of high-quality 2D seismic reflection profiles, together with 19 exploration boreholes, and published velocity models (figures 1c and 2a).

3.1.1) Exploration boreholes and dredged samples

All the available boreholes are located in the proximal part of the margin (figures 1c and 2a). *Gallastegui et al.* (2002), *Cadenas & Fernández-Viejo* (2017) and *Zamora et al.* (2017) showed seismic to well ties and described the stratigraphy of several boreholes. In this study, we used the geological and geophysical information provided by *Cadenas and Fernández-Viejo* (2017). These authors relied on velocity surveys, check-shots, sonic logs, vertical seismic profiles and available time-to-depth charts to tie the boreholes with the seismic reflection profiles (figure 2a).

18 wells were drilled within the southernmost part of the continental platform, providing stratigraphic and time constraints through the entire sedimentary cover, from Palaeozoic to Lower Miocene (figure 2a and b). Within the Asturian Basin, borehole Mar Cantábrico-H1X drilled a Mesozoic sequence, including deposits from Hauterivian to Upper Cretaceous (figure 2a and b).

No drillholes are available within the Le Danois High. Direct samples were dredged on its northern slope (*Capdevila et al.*, 1980; *Malod et al.*, 1982). Within the abyssal plain, DSDP-118 and 119 were drilled in the western corner of the Bay of Biscay (*Laughton et al.*, 1971) (figure 1c). However, direct samples are not available within the Biscay abyssal plain in the central North Iberian margin.

3.1.2) The CS-01 2D seismic reflection lines

TGS-Nopec acquired this dense mesh in 2001, corresponding to the most modern 2D multichannel seismic profiles within the area. *Cadenas and Fernández-Viejo* (2017) provide a table summarizing the acquisition and processing parameters of the reflection data. In this study, we focus on the analysis of 24 N-S and 5 E-W trending lines. This dataset provides a good data coverage and

seismic imaging of the sedimentary cover within the continental platform and slope, with 3 N-S profiles reaching the abyssal plain (figure 1d). Figures 3a, 4a, 5a, 6a, and 7a display four representative lines. Profiles CS01-124 (figure 3a), CS01-132 (figure 4a) and CS01-146 (figure 5a) run from south to north, and profile CS01-104 runs from west to east (figures 6a and 7a). Figures 3b, 4b, 5b, 6b, and 7b show the analysis of the reflectivity patterns and the seismic to well ties for each of the four representative seismic profiles. The seismic record is of a good quality up to 4-5 s TWT within the continental platform (e.g., figures 3b and 6b), and up to 6 s TWT within the Asturian Basin (e.g., figures 4b) and around the Lastres, Llanes and Torrelavega canyons (e.g., figures 5b and 7b). In the Le Danois High, reflections are coherent in the upper 2 s TWT (e.g., figure 4b). The continental slope includes coherent reflectivity in the upper part, which decreases downwards (e.g., figures 3b and 4b). The abyssal plain is highly reflective down to 9 s TWT (e.g., figure 3b and 4b). Moho reflections are not identified. This confirms that the Moho is not traceable or very limited in reflection profiles at the central part of the North Iberian margin (e.g., *Álvarez-Marrón et al*., 1996; *Fernández-Viejo et al*., 2011; *Cadenas & Fernández-Viejo*, 2017).

3.1.3) Published velocity models

In this study, we used 6 published velocity models (figure 1c). Profile ESCIN-4 is from *Fernández-Viejo et al.* (1998) and the MARCONI-1/4/5/6/8 models are from *Ruiz* (2007) and *Ruiz et al.* (2017). These models identified a surface, which shows velocity changes typical of the crust-mantle boundary, defining the refraction Moho.

3.2) Methods

We used a tectono-stratigraphic approach based on combined geological and geophysical interpretations to identify and describe Mesozoic rift basins and bounding structures, the related crustal domains, and the major Alpine compressional structures.

The identification of rift-related basins and major structures relied on borehole-constrained seismic interpretation. This allowed the recognition of the main seismo-stratigraphic units and their definition as tectono-stratigraphic units describing the Mesozoic extension and the Alpine compression (*Gallastegui et al.*, 2002; *Cadenas & Fernández-Viejo*, 2017; *Cadenas et al.*, 2018). Figure 2a shows the age constraints, the formation tops, the seismic to well ties, and the interpreted tectono-stratigraphic units along four representative boreholes. We defined the pre-/syn- and post-kinematic units, which developed prior, during, and after active rifting within a given domain, and the syn-orogenic and post-orogenic units. Within the continental platform, well log-based stratigraphy enabled the definition of all these units (*Cadenas & Fernández-Viejo, 2017*; *Zamora et al.*, 2017; *Cadenas et al.*, 2018). Within the Asturian Basin, borehole Mar Cantábrico-H1X allowed us to date the post-kinematic and the upper part of the syn-kinematic unit. Seismic facies correlation with the age-constrained seismo-stratigraphic units identified within the continental platform enabled to estimate the age of the pre-kinematic unit and the syn- and post-orogenic units (*Cadenas & Fernández-Viejo*, 2017). Within the Le Danois High, we have tentatively dated the tectono-stratigraphic units by seismic facies correlation with the borehole-constrained interpretation developed within the continental platform and in the Asturian Basin. The dredged samples on the northern slope of the Le Danois High (*Capdevila et al.*, 1980; *Malod et al.*, 1982) and the ages of samples of granulites (*Fügenschuh et al.*, 2003) have enabled to discuss the age of the Mesozoic and the Cenozoic sediments. Within the Biscay abyssal plain, the lack of drilling constraints precludes accurate age estimations, thus time constraints are tentative and based on relative correlation with the continental platform.

To constrain the crustal structure, and considering that the reflection Moho is not traceable, we gridded the refraction Moho in depth and in time from published velocity models (figure 1c). With these data, we defined and/or calculated the two-way travel time and we extrapolated this surface on to the seismic profiles. Based on the integration of the refraction Moho within the seismo-stratigraphic interpretations, we built geological cross-sections for the four representative lines (figures 3c, 4c, 5c, 6c, and 7c).

The geological interpretations allowed us to define the syn-kinematic units as syn-rift units. Syn-kinematic refers to sedimentary packages that are deposited in a tectonically active setting, while syn-rift corresponds to sedimentary units that have been deposited during a particular period of active rifting. Thus, it locally corresponds to a syn-rift unit within a given domain but it can pass laterally to a pre- or post-kinematic unit. We traced and gridded the base and the top of the two major syn-rift units (figures 8a, b and c, and 9a, b, and c) in order to develop depth and thickness maps (figures 8d, e, and 9d, e).

From this tectono-stratigraphic analysis, we extracted the information to make structural maps that illustrate the spatial distribution, the geometry and the architecture of the rift basins and bounding structures (figures 8f and 9f), enabling the definition of distinctive rift systems (figure 10a and b).

4) Crustal structure and basin architecture in the central North Iberian margin

4.1) Section CS01-124 (figure 3)

The CS01-124 profile runs across the central North Iberian margin from south to north between 5.3º´W and 5.6º´W and 43.5ºN and 44.5ºN (figure 1c).The profile crosses a continental platform 25 km wide, with a water depth of about 163 m, and a long and gently dipping continental

slope, with water depths varying from 163 m at the shelf break to about 4500 m towards the Biscay abyssal plain (figure 3a). We have distinguished four main geological sectors (figure 3c).

The southernmost sector, spanning from SP 2600 to SP 1480, is characterized by the presence of a thick cover overlying the Palaeozoic basement (figure 3c). The sedimentary record on this sector lies onto three major crustal blocks, which are 5 s TWT thick (equivalent to about 20 to 15 km, according to *Cadenas et al.*, 2018). Three major north-dipping high-angle normal faults bound these blocks, showing a top basement vertical throw of 3 s, 0.5 s, and 1.1 s TWT respectively. These faults decouple at the brittle/ductile transition, which is located between 6 s and 7 s TWT, and bound classical half-graben and graben-type basins, that we refer to as Gijón-Ribadesella depocentres. An outstanding reflection of high amplitude delineates the top of seismic basement (A in figure 3b). Between SP 2600 and 1800, the Lower to Middle Jurassic unit corresponds to the lowermost reflective level (figures 2 and 3b, borehole Asturias-D2-Bis). This unit and the overlying Late Jurassic to Barremian correspond to post-kinematic units that lie directly on top of the seismic basement between SP 1800 and SP 1500. It includes an upper reflective unit, ascribed to the Barremian, and a lower unit with reflectivity decreasing downwards, spanning from Late Jurassic to Barremian (borehole Asturias-D2 Bis, figures 2 and 3b and c). The parallel-layered Aptian to Albian and Upper Cretaceous to Middle Eocene post-kinematic units are unconformably overlain by fan-shaped Upper Eocene to Lower Miocene syn-orogenic deposits and a parallel and thin post-orogenic unit. *Gallastegui et al*. (2002) and *Cadenas and Fernández-Viejo* (2017) ascribed this unit from Middle Miocene to Quaternary (borehole Asturias-D2 Bis, figures 2 and 3c). Transparent bodies corresponding to diapirs disrupt the sedimentary record (e.g. SP 220, SP 1950, SP 1700, figures 3b and c).

The second sector spans from SP 1480 to around SP 900. At SP 1480, its southern limit corresponds to the break-away (BR-BB) of a detachment fault, named Biscay Detachment (BD). This structure has a large sub-horizontal fault offset and creates a new depositional surface (figure 3c). Over the BD, a thick post-Barremian syn-kinematic unit, tentatively dated from Aptian to Late

Cretaceous by seismic correlation (figure 3c), fills a deep and wide depocentre, showing wedge-shaped and onlap geometries onto the detachment surface. This extensional detachment fault marks a sharp deepening of the top basement from 2s to 4.5 s TWT. Around SP 1150, a change in the basement morphology from upward to downward concave describes an exhumed and dome-shaped structure that corresponds to a new detachment fault, named Biscay Detachment-1 (BD-1). The BD-1 deepens from 4.5 s TWT down to 8 s TWT, showing a large sub-horizontal fault offset. It creates a new depositional surface, which shows an irregular upward-downward-upward concave morphology. Between SP 1000 and SP 1050, it sharply deepens from 5 s TWT to 7 s TWT, marking a strong crustal thinning. On this area, two prominent high amplitude reflections (B1 and B2 in figure 3b) delineate a structural high, interpreted as an extensional allochthon. Parallel and flat reflections flooring this high delineate the detachment surface. The highest point marks the break-away (BR-BB-2) of a new detachment fault, named Biscay detachment-2 (BD-2), which corresponds to the southern limit of the third sector.

The third sector spans from SP 900 to SP 600. The BD-2 deepens from 8 s to 9.5 s TWT delineating a dramatic crustal thickness reduction. The sedimentary infill thickens progressively oceanwards and shows chaotic and incoherent reflectivity patterns. It represents a tectonized area due to Alpine reactivation.

In the fourth sector, a thick post-orogenic unit wedging out at the toe of the slope covers the backstop of the Biscay Accretionary Wedge. A major north-directed thrust (reflection C in figure 3b), named Biscay Thrust-2 (BT-2), and a south-directed back thrust (reflection D in figure 3b) control the geometry of the thrust sheet, which describes a 15 km wide gentle anticline. It includes a thick syn-orogenic unit unconformably overlying the parallel-layered pre-orogenic and post-kinematic unit. *Álvarez-Marrón et al.* (1997) ascribed the post-orogenic unit from Upper Miocene to Quaternary, the syn-orogenic unit from Middle Eocene to Middle Miocene, and the pre-orogenic and post-kinematic from Upper Cretaceous to Palaeocene, based on correlations with the stratigraphic record of

DSP-118 and 119 wells, located at the western corner of the Bay of Biscay (*Laughton et al.*, 1971) (figure 1c). At the base of the cover, a thick late Cretaceous syn-kinematic wedge, tentatively ascribed from Aptian to Late Cretaceous, shows onlap geometries landwards. The Biscay Thrust-2 (BT-2 in figure 4c) and a back-thrust bound this package and sole out at 10 s TWT.

4.2) Section CS01-132 (figure 4)

The profile CS01-132 runs across the central North Iberian margin from south to north between 4.8ºW and 5.1ºW and 44.5ºN and 43.5ºN (figure 1c). The profile crosses a narrow continental platform 20 km wide, with water depths of about 172 m, the 35 km wide Asturian Basin, with water depths up to 1000 m, shallowing again up to 490 m towards the Le Danois High, which delineates the shelf break (figures 4a). The short and steep continental slope finishes at 4500 m of depth towards the Biscay abyssal plain. Four main sectors have been distinguished (figure 4c).

The southern sector, spanning until SP 600, is depicted by the presence of a thick Upper Eocene to Lower Miocene syn-orogenic wedge, which onlaps progressively onto uniform parallel-layered and continuous Late Cretaceous to Palaeocene post-kinematic and pre-orogenic sediments (borehole Mar Cantábrico C4, figures 2 and 4b and c). These include a well-defined Upper Cretaceous to Palaeocene upper unit 0.5 s TWT thick, and a uniform Aptian to Albian lower unit 1 s TWT thick (boreholes Mar Cantábrico-H1X and Mar Cantábrico-C4, figures 2 and 4b and c). The upper crust lies onto a lower crustal level including outstanding short and bright reflections identified between 7 s and 9 s TWT southwards of SP 500 (figure 4b).

The second sector, spanning from SP 600 to SP 1400, corresponds to the Asturian Basin. The F1 and F2 planar and high-angle faults (*Cadenas and Fernández-Viejo*, 2017) delimit the depocentre and show a top basement vertical throw of about 2 s and 1 s TWT respectively (figure 4c). They penetrate the lower crust and sole out at the base of the crust at 9.5 s TWT, without offsetting the

top of the mantle (Moho). The Asturian Basin developed on top of a crustal domain less than 3 s TWT thick (figure 4b), (e.g., 11 km, *Cadenas et al.*, 2018). The base of the sedimentary cover corresponds to a continuous and outstanding Lower to Middle Jurassic pre-kinematic unit 0.5 s TWT thick. This basal level is unconformably overlain by a thick wedge of Late Jurassic to Barremian syn-kinematic deposits (borehole Mar Cantábrico-H1X, figures 2 and4b and c). It includes a rather transparent lower level of variable thickness, consisting of Late Jurassic to Barremian sediments, and a more uniform upper level showing a regular and less variable thickness, ascribed to the Barremian, with reflectivity increasing upwards (borehole Mar Cantábrico-H1X, figures 2,4b and c). This unit is covered by the parallel-layered and continuous Aptian to Middle Eocene post-kinematic and pre-orogenic unit. It includes an Aptian to Albian lower level 1 s TWT thick and a well-imaged Upper Cretaceous to Palaeocene upper level. Four reflections of high amplitude bound these two units (A, B, C and D in figure 4b). Fan-shaped Upper Eocene to Lower Miocene syn-orogenic sediments, which are floored by a highly reflective erosional truncation (e.g., E in figure 4b), lie unconformably on top of the pre-orogenic units. A well-defined angular unconformity underlies the tabular and sub-horizontal Upper Miocene to Quaternary post-orogenic unit. Anticlinal structures cored by inverted normal and minor reverse faults affected the upper syn-kinematic unit. They resulted in the uplift and erosion of the post-kinematic units and controlled the geometry of the syn-orogenic units. Two major hanging-wall anticlinal structures can be observed at the edges of the basin at SP 500 and SP 1400, due to the inversion of the two major bounding faults (e.g., F1 and F2 faults), which are accompanied by several splay faults (figure 4c). At the central part of the basin, the inversion of north-verging and south-verging structures gave place to the uplift of a gentle anticline (SP 1000, figure 4c).

At SP 1400, the break-away of a detachment fault (BR-LD) marks the southern limit of the third sector, spanning between SP 1400 and SP 2100 (figure 4c), which corresponds to the Le Danois acoustic basement block. This block shows a maximum crustal thickness of 5 s TWT, equivalent to about 20 km (*Cadenas et al.*, 2018). We call the extensional detachment the Le Danois

Detachment (LD). The LD deepens from 1.8 s to 3 s TWT and forms the top of an over-tilted block preserving pre-rift sediments at its southern border, which is interpreted as a break-away block of the LD (figure 4c, SP 1400). At SP 1500 and 1700, two structural highs floored by flat reflections can be interpreted as extensional allochthons. The highest points correspond to the break-away (e.g., BR-LD-1 and BR-LD-2) of two detachment faults, the Le Danois Detachment-1 and the Le Danois Detachment-2 (e.g., LD-1 and LD-2 in figure 4c). These structures show upward to downward concave geometries, representing dome-shaped exhumed surfaces. Post-Barremian syn-kinematic units, tentatively ascribed from Aptian to Late Cretaceous based on seismic correlations, overlay the exhumed detachment surfaces (figure 4c). These syn-kinematic sediments show wedge-shaped structures onlapping onto the over-tilted blocks preserved in the footwall and onto the extensional allochthons. They display north(ocean)ward downlapping geometries onto the exhumed detachment surfaces (e.g., between SP 1500 and 1700 in figure 4c). Late Cretaceous to Eocene post-kinematic units cover the BR-LD break-away. The sedimentary cover, the allochthon blocks and the underlying detachment faults are tilted towards the south and progressively uplifted, eroded, and unconformably overlain by the syn-orogenic and the post-orogenic units towards the top of the Le Danois High.

The Le Danois Thrust (LDT)marks the southern limit of the fourth sector, which occupies the Biscay abyssal plain (figure 4c). Within this sector, the thick parallel-layered and horizontal post-orogenic unit wedges out at the toe of the slope and overlies the Biscay accretionary wedge. The wedge includes a syn-orogenic unit on top of a parallel-layered pre-orogenic level, which have been ascribed from Middle Eocene to Middle Miocene and from Upper Cretaceous to Palaeocene (*Álvarez-Marrón et al*., 1997). Two thrust sheets occur in the hanging wall of two major north-directed thrusts, named Biscay Thrust and Biscay Thrust-2 (BT and BT-2 in figure 4c). The Biscay Thrust (reflection G in figure 4b) limits the northern thrust sheet up to 8.5 s TWT. Within this thrust sheet, minor thrusts affect the pre-orogenic and post-kinematic unit and the thick syn-kinematic units, which fill the Biscay depocentres. We tentatively ascribe the syn-kinematic units from Aptian to Late

Cretaceous. These units overlie a well-imaged reflection of high amplitude delineating the top basement (e.g., H in figure 4b). This sub-horizontal surface runs between 9 and 10 s TWT and is interpreted as an extensional detachment surface (Biscay Detachment Surface in figure 4c). The thrusts disrupt this surface, soling out between 10 s and 11 s TWT. The Biscay Thrust-2 bounds the southward thrust sheet up to 7 s TWT. This sheet is emplaced at shallower levels and represents a highly deformed area imaged by complex and diffuse structural patterns. We interpret in this area a well-defined syn-orogenic mass-wasting deposit and a tectonized area in which we define a highly deformed syn-kinematic unit on top of tilted blocks.

4.3) Section CS01-146 (figure 5)

The profile CS01-146 runs at the central North Iberian margin between 44.1ºN and 43.3ºN and 3.6ºW and 4.5ºW (figure 1c). It crosses a short continental platform 8 km wide, with water depths of about 110 m, and the deep and wide slopes of the Lastres and Torrelavega canyons, with water depths reaching about 2400 and 2900 m respectively and ending into the Biscay abyssal plain area at about 3980 m of depth (figure 5a). This section includes three main sectors (figure 5c).

The southernmost sector spans from SP 2200 until SP 1500. At SP 2000, the basement deepens from 4 s to more than 5 s TWT, marking a structural high. We interpret this high as the break-away (BR-LLD-1) of a detachment fault named Llanes Detachment (LLD-1 in figure 5c). Some reflections of high amplitude can be traced between 7s and 7.5 s TWT (figure 5b), which are interpreted as the brittle-ductile transition (figure 5c). The BR-LLD-1 point is covered by short, discontinuous and incoherent reflections at around 4 s TWT (e.g., A in figure 5b), which delineate the base of wedge-shaped syn-kinematic, ascribed from Aptian to Late Cretaceous. A thick Late Cretaceous to Middle Eocene post-kinematic unit is unconformably overlain by bodies of incoherent and chaotic reflections (figure 5b), corresponding to the Upper Eocene to Lower Miocene syn-

orogenic units (figure 5c). Minor thrusts control the geometry of the fan-shaped syn-orogenic units, which are related to the activity of the Llanes and Torrelavega canyons.

At SP 1500, a prominent structural high marks a basement deepening from 4.5 s to 6.5 s TWT and the southern limit of the second sector, spanning from SP 1500 to SP 700. We interpret this high as the break-away point (BR-LLD-3 in figure 5c) of a detachment fault, named Llanes Detachment-3 (LLD-3 in figure 5c). Within this sector, other three prominent structural highs can be recognized (figure 5b). All these asymmetric structural highs and their related highest points correspond to extensional allochthons and the break-away point (BR-LLD-4, BR-LLD-5, BR-LLD-6 in figure 5c) of different, in-sequence extensional detachment faults, the Llanes Detachment-4, the Llanes Detachment-5, and the Llanes Detachment-6 (LLD-4 and LLD-5 in figure 5c). High amplitude, short, discontinuous, and flat reflections image the detachments (B in figure 5b), delineating the top of seismic basement (figure 5c). These structures deepen progressively from 6 s to 8 s TWT, flooring extensional allochthons. Syn-kinematic wedges thickening oceanwards, cover these blocks (figure 5c). High amplitude reflections (A in figure 5b) separate the syn-kinematic wedges and a thick sub-horizontal post-kinematic unit. Between SP 1800 and 1500, these units are uplifted and tilted towards the south due to the emplacement of a south-dipping thrust (e.g., Llanes Thrust-LLT- in figure 5c) on top of the crustal block related to the LLD-3. Southwards of SP 1500, an erosional truncation imaged by short and high amplitude reflections (C in figure 5b) floors thick syn-orogenic and post-orogenic units. Between SP 900 and SP 700, the syn-kinematic and the post-kinematic units are tilted towards the south and describe a gentle anticline related to the emplacement of a north-directed thrust (Torrelavega Thrust-TT-, figure 5c).

The third sector spans from SP 700 to SP 100. Reflections delineating the top of seismic basement (B in figure 5b) deepen from 7 s to 8.5 s TWT. At SP 700, the syn- and the post-kinematic units describe a gentle anticline onto a rather transparent area. We relate the basement deepening to the break-away (BR-LL-7) of a new detachment, named Llanes Detachment-7 (LLD-7 in figure 5c).

This structure shows upward to downward concave and irregular geometries. An allochthon block lies on top of the flat reflections (B in figure 5b) delineating the LLD-7. This block was uplifted and tilted due to the emplacement of a north-directed thrust, named Torrelavega Thrust (TT). The syn- and post-kinematic units lying onto the hanging-wall of the LLD-7 describe a gentle north-verging anticline related to the reactivation of the LLD-7 as a back-thrust. Within this sector, two minor structural highs are interpreted as allochthons with the highest point corresponding to the break-away point (BR-LLD-8 and BR-LLD-9 in figure 5c) of the Llanes Detachment-8 and Llanes Detachment-9 (LLD-8 and LLD-9 in figure 5c). An up to 4 s TWT thick syn-kinematic unit pinches out towards the detachment faults. These sediments show onlap geometries onto the allochthons and downlapping geometries oceanwards (e.g., between SP 500 and 100 in figure 3b and c). This unit is covered by a sub-horizontal and thick post-kinematic unit. An erosional truncation (C in figure 5b) floors the upper part of the sedimentary record, which includes superimposed packages of parallel-layered reflections corresponding to the syn- and post-orogenic units related to the activity of the Santander canyon.

4.4) Section CS01-104 (figures 6 and 7)

The profile CS01-104 runs across the central North Iberian margin between 43.7ºN and 43.9ºN (figure 1c). It spreads 125 km over the continental platform, with water depths of about 120 m (figure 6a). It transects the complex system of the Lastres and Llanes submarine canyons, deepening until 1630 m, and the Torrelavega canyon, deepening until about 2800 m (figure 7a). We distinguish four structural segments (figures 6c and 7c).

Within the westernmost segment, spanning from SP 5500 until SP 7700, discontinuous reflections of high amplitude (A in figure 6b) delineate the top of seismic basement between 3 s and 4 s TWT (figure 6c). West-directed high-angle and listric normal faults disrupt the top of seismic basement. These domino faults are decoupled in the brittle/ductile transition at around 7 s TWT and

separate out distinctive tilted crustal blocks and overlying half-grabens, corresponding to the Gijón-Ribadesella depocentres (figure 6c). The base of the sedimentary infill shows a rather transparent level including Triassic evaporites (borehole Asturias-D2 Bis, figures 2 and 6b and c). This unit thickens into the footwall of the listric normal faults, resulting in the formation of restricted aggradational syn-kinematic units and half-graben geometries (e.g., figures 6b and c, between SP 5500 and SP 6000).

A highly reflective and uniform Lower Jurassic to Middle Jurassic post-kinematic unit is locally imaged overlying these levels (e.g., around SP 5500, SP 6500, figures 6 b and c). The sedimentary infill includes almost isopach, parallel-layered and continuous Upper Jurassic to Barremian, Aptian to Albian and Late Cretaceous to Middle Eocene units. Three reflections of high amplitude delimit these units (B, C, and Din figure 6b). Transparent and chaotic bodies corresponding to diapirs disrupt the sedimentary record (e.g. SP 6000, SP 7000 and SP 8000 in figure 6b). These bodies control the shape and the extent of the Upper Eocene to Oligocene syn-orogenic wedges, which are capped by a highly reflective erosional truncation (D in figure 6b). At SP 7700, an abrupt deepening of the top of seismic basement from 2.5 s to 5 s TWT marks the southern limit of the second sector (figure 6b), which is related to a high-angle and listric normal fault (Ayalga Fault, figure 6c). This fault shows a dip-slip offset of the top of seismic basement of about 3 s TWT and decouple at the base of the crust at around 8 s TWT (figure 6c). Within this sector, short and discontinuous reflections of high amplitude (A and A´) delimit a highly reflective and homogeneous Lower to Middle Jurassic pre-kinematic unit. This unit is 0.5 s TWT thick and it delineates the base of the sedimentary infill, which draws a deep depocentre, corresponding to the Asturian Basin (figure 6c). The Upper Jurassic to Barremian syn-kinematic level thickens dramatically, showing a maximum thickness of about 3 s TWT (figure 6c). It includes an Upper Jurassic to Hauterivian lower level showing poor reflectivity and an almost isopach Barremian upper level, including short and parallel reflections (figure 6b). The post-kinematic unit includes an Aptian to Albian level of about 1.5 s TWT

thick and Upper Cretaceous to Eocene level 0.5 s TWT thick. The upper post-kinematic unit is truncated by a prominent unconformity delineating the base of the syn-orogenic unit (D in figure 6b).

At SP 10000, the top of seismic basement shallows until 3.5 s TWT, linked to a high-angle normal fault (Xana Fault in figure 7c), which corresponds to the northern limit of the third sector. This structure shows a dip-slip offset of the top of seismic basement of about 2 s TWT and a related roll-over anticline, and decouples at the base of the crust at around 9 s TWT (figure 7c). The Xana Fault is reactivated and shows a related anticline, and a splay west-dipping reverse fault. We interpret the transparent and chaotic seismic facies identified around the Xana Fault as a diapir. Within the third sector, the seismic basement includes sub-parallel highly reflective levels, which are located between 3 s and 5 s TWT. We interpret these surfaces as the intersection of north-dipping extensional detachment faults of the Llanes Detachment System (LLD-1, LLD-2, and LLD-3 in figure 7c) and north-directed thrusts. These levels deepen progressively towards the east, and are disrupted by west-dipping thrusts (e.g., SP 11500 in figure 7c). The sedimentary cover includes a syn-kinematic unit 0.5 s TWT thick, which we tentatively date from Aptian to Late Cretaceous by seismic facies correlation. The Late Cretaceous to Eocene post-kinematic unit is unconformably overlain by thick syn- and post-orogenic units, which are transected by the Lastres canyon (figure 7c).

Between SP 12000 and SP 13000, at the limit between the third and the fourth sectors, the intersections of the LLD-1 and the LLD-2 deepen until 7 s TWT. Two outstanding and sub-parallel reflections of high amplitude (E and F in figure 7b) truncate these surfaces. We interpret the reflections as two major east-dipping thrusts (e.g., Lastres Thrust-1-LT-1- and Lastres Thrust-2-LT-2- in figure 7c). The LT-2 delineates the top of seismic basement within the fourth sector. The thrusts cut highly reflective levels that we assign to locally preserved Lower Jurassic to Barremian pre-rift sediments (e.g., SP 13500 and 15000 in figure 7c) and intersections of reactivated north-dipping extensional detachment faults (e.g., SP 14500 in figure 7c). The sedimentary cover includes a thick syn-kinematic unit that we tentatively ascribed from Aptian to Late Cretaceous. This unit thickens

dramatically towards the east until reaching 2.5 s TWT. The Late Cretaceous to Eocene post-kinematic unit thickens as well towards the east and is unconformably overlain by thick syn- and post-orogenic units, which is transected by the Llanes and Torrelavega canyons (figure 7c).

5) Rift systems within the North Iberian-Bay of Biscay rift

The multi-stage North Iberian rift can be described as a complex patchwork of three overprinting rift systems. They show a different rift template and kinematic framework and they include syn-kinematic units of different age that belong to three different syn-rift units

5.1) The diffuse Triassic Gijón-Ribadesella rift system

The Gijón-Ribadesella rift system includes the Gijón-Ribadesella depocentres, which are filled by a Triassic syn-rift unit 1(figure 2, 3c and 6c). NW-SE and NE-SW trending high-angle and listric extensional faults accommodated relatively small amounts of extension, including distributed stretching and minor and localised crustal thinning. This resulted in a limited vertical increase of accommodation space and the formation of half-graben-type, syn-kinematic depocentres of Triassic age. These depocentres developed in between tilted blocks, overlying weakly thinned crust (figure 3c).

The Gijón-Ribadesella system shows a low-β architecture (e.g., *Wilson et al.*, 2001, *Tugend et al.*, 2015) (figure 10a), as observed in the North Sea rift system (*Cowie et al.*, 2005). Structural variations within the Gijón-Ribadesella system (figures 3c and 6c) can be related to different phases leading to incipient localisation of deformation and structuration of the rift system, as it has been recognized in the northern North Sea *(Bell et al*., 2014; *Phillips et al*., 2019; *Schiffer et al.*, 2019).

5.2) The narrow and localised Late Jurassic to Barremian Asturian rift system

The Asturian rift system includes depocentres with an Upper Jurassic to Barremian syn-rift unit-2 and Aptian to Middle Eocene post-kinematic units. Within the studied zone, this is the case of the Asturian Basin (figures 2, 4c and 8b). Between 5º15´W and 4º50`W, the *base of the Upper Jurassic to Barremian* sedimentary contact draws a pronounced graben that reaches 6600 ms TWT and shallows again to 1500 ms TWT towards the edges (figure 8d). The Upper Jurassic to Barremian syn-rift unit 2 thickens abruptly within the basin, showing a maximum thickness of about 4000 ms TWT (figure 8e). The F1, the F2, the Ayalga, and the Xana faults delimit the extreme thickening of this unit (figure 8e). The planar and high-angle F1 and F2 bounding faults show minor dip-slip offsets of the top of seismic basement, juxtaposing crusts and sediments of highly different nature and thickness. Thus, we interpret these structures as master strike-slip faults (figure 4c and 8f). The Ayalga and Xana faults show greater dip-slip offsets and listric geometries and they juxtapose crust and sediments of different thickness, showing roll-over structures in the hanging-wall. Thus, we interpret these structures as high-angle normal faults (figure 6c and 8f). The bounding faults accommodated high degrees of crustal thinning, resulting in the formation of a restricted and laterally confined thinned domain (figure 8e and f). The basin shows a lozenge shape, occupying an area of 689 km^2 (figure 8f). It displays a maximum width of 25 km and a maximum length of 36.8 km, with the largest diagonal of about 42 km in a NE-SW direction and a shortest diagonal of about 34 km in a NW-SE direction.

The Asturian Basin shows all the characteristics of a confined pull-apart basin, corresponding to a rhomboidal releasing bend, which developed within a transtensional or oblique rift system (e.g., *Morley et al.*, 2004; *Mann*, 2007), such as the Dead Sea Basin (e.g., *Smith et al.*, 2008). The observed structural features are compatible with a sinistral sense of shear. Consequently, we suggest that the Asturian Basin correspond to a left-lateral pull-apart basin, accommodating extension

by partitioning of deformation between the master F1 and F2 left-lateral strike-slip and the Ayalga and Xana dip-slip faults.

5.3) The deep and wide Aptian to Cenomanian Biscay rift system

The Biscay System includes the Biscay depocentres, which are filled by the Aptian to Cenomanian syn-rift unit 3 (figure 9a, b, and c). Within these depocentres, the Triassic and the Upper Jurassic to Barremian sediments are part of the pre-kinematic unit, which is only preserved in extensional allochthons (figure 9a, b, and c). The *base of the Aptian to Cenomanian syn-rift unit 3* is delineated by distinctive extensional detachments of the Biscay, the Le Danois, and the Llanes detachment systems (figures 9a, b, and c). The southernmost Biscay Break-away point (BR-BB in figure 9d), Le Danois Break-away point (BR-LD in figure 9d), and Llanes Break-away point (BR-LL in figure 9d), mark the abrupt deepening and thickening of this unit (figure 9d and e). Despite the partial underthrusting and/or reworking and the uplift, tilting and erosion of part of this unit due to the emplacement of north-directed thrusts (e.g. the LDT, the BT, the BT-2, the TT, in figure 9a, b, c, and e), it shows former thickness variations between 1800 and 3600 ms (figure 9e). Eastwards of 4º40' W, it spreads across the whole margin and shows an abrupt thickening in two major depositional areas, showing a maximum thickness of 3300 ms and 4500 ms respectively (figure 9e).

The BR-BB, the BR-LD, and the LL-BR break-away lineaments delimit and bound two v-shaped domains within the Biscay rift system: the Biscay/Le Danois system and the Llanes system (figure 9f). These lineaments mark the initiation of crustal thinning, corresponding to the proximal limit of the necking zone (Mohn *et al.*, 2014) (figure 9a, b, and c). Based on the recognition of the Biscay Detachment surface delineating the top of seismic basement between 9s and 10s TWT (e.g., reflection H in figure 4b), we interpret that the basement within the abyssal plain corresponds to exhumed and serpentinized mantle. Published velocity models (*Fernández-Viejo et al.*, 1998; 2012;

Ruiz et al., 2017) and gravity inversion results (e.g., *Tugend et al.*, 2014) support this interpretation. Consequently, we conclude that the Biscay Detachment System led to extreme crustal thinning and mantle exhumation at the northern edge of the Biscay domain (figure 9a and b). The presence of a sub-horizontal extensional detachment surface (reflection C in figure 5b) marking the to the top of seismic basement at around 8 s TWT, with overlying allochthon blocks, suggests that, at the north-eastern corner of the Llanes domain, the basement consists of exhumed and serpentinized mantle. Thus, we suggest that the Llanes Detachment System may also have resulted in mantle exhumation much further to the south (figure 9c).

The Biscay/Le Danois and the Llanes systems clearly represent so-called *high-β* settings (e.g., *Wilson et al.*, 2001; *Tugend et al.*, 2015), also referred to as hyperextended rift systems (e.g., *Whitmarsh et al.*, 2001; *Péron-Pinvidic et al.*, 2013). The Biscay, Le Danois, and Llanes extensional detachment systems accommodated crustal necking and hyperextension processes, resulting in the creation of large sub-horizontal accommodation space and the formation of the sag-type Biscay depocentres (figure 10a). The break-away lines of the three detachment systems display a distinctive and irregular trend (figure 10b), suggesting that the Biscay/Le Danois and the Llanes systems may have developed with different kinematics and/or as compartmentalized segments of a propagating rift system. Segmentation within hyperextended rift systems has been related either to transfer zones (e.g., *Lister*, 1986; *Tugend et al.*, 2014; *Nirrengarten et al.*, 2018) or to relay zones (*Lescoutre and Manatschal*, 2020). The abrupt variation in the trend of the BR-LD and the BR-LL lines and in the width of the Biscay/Le Danois and the Llanes domains occurs across the so-called Santander Transfer Zone (*Roca et al.*, 2011) (figure 9f). On a map scale, we observe that the Biscay/Le Danois system wedges out eastwards, while the Llanes system widens abruptly in a N-S direction (figure 9f). According to our interpretation, the so-called Santander Transfer Zone corresponds to a relay within evolving segmented hyperextended rift systems.

6) Discussion

6.1) Poly-phase vs multi-stage rift systems

It has been widely accepted that the architecture of rifted margins results from poly-phase rifting (figure 10c and d). Poly-phase rifting corresponds to a unique rift event, which develops through successive rift phases during progressive, active, and dynamic migration and localisation of deformation from stretching, to thinning, to exhumation, to seafloor accretion with the same kinematic framework (*Lavier and Manatschal*, 2006). Poly-phase rifted margins include in-sequence rift structures and syn-tectonic units, which are progressively younging oceanwards (e.g.; *Péron-Pinvidic et al.*, 2013; *Ribes et al.*, 2019) (figure 10c). The structure of such poly-phase rifted margins can be described in terms of rift domains, corresponding to coherent and genetically linked structural domains and bounding rift structures (e.g., *Tugend et al.*, 2015) (figure 10c and d). Multi-stage rifting implies, however, distinctive rift events, which result into the spatial overlap of distinctive rift systems (figure 10b). Each rift system is characterized by its age, kinematics, and a rift architecture (figure 10a and b). Consequently, the use of the rift domain approach is challenging in multi-stage rift systems. This work shows that description of the architecture of multi-stage rift systems mainly requires the identification of major rift basins, their bounding rift structures, and the syn-rift units, together with related crustal domains (figure 10a and b). It enables to distinguish among genetically linked structural domains belonging to the same rift system, and to define their spatial distribution and overprint (figure 10a and b). This approach, discussed on this paper, allows to define, map, and describe the complex rift systems forming the North Iberian margin and to explain the yet poorly understood margin architecture. Our results enable to conclude that the North Iberian margin corresponds to a multi-stage rift rather than to a poly-phase rift system.

An analysis of the map showing the distribution of the Gijón-Ribadesella, the Asturian, and the Biscay rift systems reveals a distinct stacking pattern of the three rift systems, in both a N-S and an E-W direction (figure 10b). Remnants of the Gijón-Ribadesella rift system are best preserved in areas with no overprint by later rift events, where the crust is >20 km thick, such as the continental platform or onshore areas (e.g., *Suárez-Rodríguez*, 1988; *Pieren et al*., 1995*; López-Gómez et al.*, 2019). The Asturian System can be found over crust <12 km thick at the central North Iberian margin. It partly overprints the Gijón-Ribadesella system and it is circumvented by the Biscay system. Previous studies have interpreted the boundary between the Le Danois Basin (Asturian Basin in this study) and the hyperextended Basque-Cantabrian Basin (e.g., *Pedreira et al.*, 2003; *Quintana et al*., 2015; *Pedrera et al.*, 2017; *DeFelipe et a*l., 2019) as part of the Santander Transfer Zone (*Roca et al*., 2011; *Tugend et al*., 2014). In this study, we define the Asturian Basin as a localised pull-apart basin with a present-day eastern termination located further west, which is, thus, not related to the hyperextended Basque-Cantabrian Basin (figure 10b). The Biscay System is widespread. It overprints the Gijón-Ribadesella rift system but circumvents the Asturian Basin. It includes at least two segments, the Biscay/Le Danois and the Landes domains, which occupy the continental slope, the abyssal plain, and part of the continental platform.

6.2) Control of inheritance on multi-stage rifting

6.2.1) Orogenic inheritance

Orogenic inheritance can effectively control the rift evolution and its final architecture (*Chenin et al.*, 2017). Basement discontinuities may play a major role during rifting, breakup and the development of transform systems (*Peace et al*., 2018). Examples are the North Sea Rift, where the Caledonian inherited structures controlled different rifting phases and distribution of deformation

(e.g., *Bell et al.*, 2014; *Phillips et al.*, 2019; *Schiffer et al.*, 2019). Within the Iberian domain, it has been proposed that Variscan and post-Variscan structures controlled the incipient Triassic rift (*Zamora et al.*, 2017; *López-Gómez et al.*, 2019). Thereby, the complex Variscan template (*Fernández-Lozano et al.*, 2019) may have influenced the diffuse distribution of high-angle faults and the incipient localisation of deformation within the Gijón-Ribadesella System during the Triassic.

Transtensional rift systems reactivate pre-existing basement fabrics striking oblique to the rift axis (e.g., *Morley et al.*, 2004). The F1 and F2 master strike-slip faults, and the Ayalga and Xana dip-slip normal faults have the same trend than major extensional faults of the same age onshore. These onshore faults have been interpreted as reactivated Variscan and/or post-Variscan structures (e.g., *Lepvrier and Martínez-García*, 1990; *Uzkeda et al.*, 2016). Thus, we speculate that major post-Variscan and Variscan structures may have played a fundamental role in the development of master strike-slip and dip-slip faults within the transtensional rift system.

The role of the inherited Variscan template during the development of the hyperextended Biscay System is less straightforward. Moreover, the Biscay System circumvents the Asturian Basin and does not seem to follow the diffuse Gijón-Ribadesella System.

6.2.2) Role of rift inheritance on subsequent rift events

The Gijón-Ribadesella rift system includes evaporite levels that belong to the syn-rift unit-1 (figures 2,3c). Consequently, salt diapirs are often related to half-graben-type rift basins (figure 3c and 6c) (*Zamora et al.*, 2017). Diapirism and halokynesis controlled the shape of the Lower to Middle Jurassic, Upper Jurassic to Barremian and Aptian to Middle Eocene post-kinematic units. Unequivocal evidence of diapirism is missing beneath the Asturian Basin (e.g., figures 3c and 6c). We have interpreted diapirs at the borders of the Asturian Basin, related to the Ayalga and Xana faults (figures 6c and 7c). One possible interpretation is that the salt was squeezed only at the borders of the

pull-apart basin, linked with the bounding faults. An alternative interpretation is that the pull-apart basin formed at the edges of the Triassic evaporites. This would explain the lack of evaporites in the basin. Onshore, Triassic deposits within the so-called Gijón-Ribadesella Basin do not contain evaporites (e.g., *Suárez-Rodríguez*, 1988; *Pieren et al.*, 1995; *López-Gómez et al.*, 2019). Within the Biscay System, the Triassic evaporites did not play a major role as decollement levels. An explanation is that the Biscay System resulted in the exhumation of new surfaces devoid of pre-kinematic Triassic evaporites. The pre-kinematic cover was rifted apart, and thus, diapirs and halokynesis-related structures could only be found on top of allochthon blocks, preserving the Triassic pre-kinematic cover (*Jammes et al*., 2010a).

The role of narrow and localised depocentres, such as the Asturian Basin, on subsequent rift events, and particularly, during the hyperextension phase, is enigmatic. The westwards break-away point of the Le Danois Detachment System and the eastward break-away point of the Llanes Detachment System can be found at the westward and eastward terminations of the Asturian Basin (figure 10b). The BR-LD lineament is located northwards of the F2 master strike-slip bounding fault and the BR-LL line runs eastwards of the F1 master strike-slip fault (figure 10b). A relay ramp between the Le Danois and the Llanes Detachment Systems developed at the eastern termination of the Asturian Basin (figure 10b). Thus, we suggest that the transtensional system might have conditioned the breaking-away of the Biscay System, without being directly reactivated.

6.3) Evolution of the multi-stage rift system in the central North Iberian margin

6.3.1) The Middle to Late Triassic rift event

López-Gómez et al. (2019) dated the onset of rifting in the Middle/Late Triassic. Upper Triassic siliciclastic sequences and evaporites, interpreted as a syn-rift unit 1 (e.g. Keuper facies) (figure 2a and 4c) filled the Gijón-Ribadesella half-graben type depocentres (figure 11).

6.3.2) Early to Middle Jurassic shallow marine platforms

During the Early and Middle Jurassic, shallow marine platforms developed throughout the whole area (figure 11). Limestones and marly limestones (borehole Mar Cantábrico-K1 and Mar Cantábrico-D1) (*Gutiérrez-Claverol and Gallastegui*, 2002; *Cadenas and Fernández-Viejo*, 2017; *Zamora et al*., 2017) (figure 2b), belonging to the well-known "Lias facies", have been classically interpreted as the "pre-rift" unit in north Iberia, with respect to the subsequent and major Late Jurassic to Late Cretaceous rift events (e.g. *Bois et al.*, 1997; *Espina*, 1997; *Vergés and García-Senz*, 2001; *Ferrer et al.*, 2008; *Quintana*, 2012; *Cadenas and Fernández-Viejo*, 2017). The fact that the unit is isopachous (e.g., figure 3c and 4c), showing a maximum thickness of about 800 m, together with its development in shallow marine environments over wide areas (*Valenzuela*, 1986; *Riaza*, 1996), suggests a general subsidence in a tectonically quiescent regime.

6.3.3) The Late Jurassic to Barremian rifting

From Late Jurassic to Barremian, the transtensional Asturian System developed (figure 11). The lack of borehole data across the whole infill precludes an accurate estimation of the onset of this event. The Mar Cantábrico-H1X borehole drilled Valanginian sediments at 4658 m (figure 2a). The Lower Jurassic to Middle Jurassic pre-kinematic unit is well-imaged at the base of the depocentre at around 13 km (*Cadenas et al.*, 2018). This would imply the deposition of a thick Upper Jurassic to Hauterivian sequence. This package corresponds to a syn-rift unit 2, which thickens dramatically

towards the depocentre, revealing a major period of transtension. The Barremian sequence is almost isopachous, denoting the termination of this event (figure 11).

6.3.4) The Late Aptian to Cenomanian rifting

From late Aptian to Cenomanian, the extensive Biscay rift system developed (figure 11). The lack of direct data precludes accurate time constraints for this period. Correlation of well-based seismic stratigraphy described in more proximal areas enabled us to ascribe the onset of rifting to Aptian. Samples of granulites into Aptian to Albian breccias were recovered at the northern slope of the Le Danois High (*Capdevila et al*., 1980; *Malod et al*., 1982). Apatite fission-track ages provided cooling ages for two samples of 138 and 120 Ma and led to the interpretation of these samples as middle to lower crustal remnants exhumed during the Lower Cretaceous rifting (*Fügenschuh et al*., 2003). Assessed on age estimations in hyperextended systems of northern Iberia (e.g., *Jammes et al*., 2010b; *Masini et* al., 2014; *Tugend et al*., 2014), we tentatively ascribe the end of rifting to Cenomanian. Thus, we define roughly a time span for syn-rift unit 3 from late Aptian to Cenomanian. Further studies and correlations between the Biscay/Le Danois and the Llanes domains are required to discern if the onset of extension occurred simultaneously in both domains or if extension initiated in the west (e.g., Biscay domain) and migrated towards the east.

6.4) Multi-stage rifting and plate kinematic context

6.4.1) Kinematic reconstructions of multi-stage rift systems

Multi-stage rifting claims for a reappraisal of present-day kinematic templates at the basis of spatial and temporal kinematic reconstructions of conjugate rifted margins. Crustal thickness estimations on conjugate margins and rift domain mapping approaches led to great advances on tight-fit plate kinematic reconstructions of the southern North Atlantic (e.g., *Nirrengarten et al.,* 2018; *Peace et al.*, 2019). This area includes major rift basins, such as the Orphan Basin (e.g., *Welford et al*., 2012; *Gouiza et al.*, 2017), the Porcupine Basin (e.g., *Reston et al*. 2004, *Watremez et al*., 2016), and the Galicia Inner Basin (e.g., *Murillas et al*., 1990; *Pérez-Gussinyé et al.*, 2003; *Sandoval et al*., 2019). However, these basins have been defined as poly-phase hyperextended rift basins, including distinctive sub-basins and different structural domains.

The existing models are unable to restore satisfactorily the architecture of the Iberian-Newfoundland and North Iberian and Armorican margins. This may be related to the fact that present-day kinematic models have not integrated yet multi-stage rift systems. Their identification and characterization (e.g., figure 10a and b) is a keystone to set up present-day kinematic templates. Multi-stage rift systems include overlapped, independent and out of sequence deformable domains, continental fragments and rift boundaries that are crucial to restore each rift system back in time and in space, minimising gaps and/or overlaps in the resulting reconstructions.

6.4.2) Multi-stage Mesozoic rifting along the Iberian/European plate boundary

The kinematic evolution of the Iberian plate during the Mesozoic and, particularly, the opening and subsequent partial closure of the Bay of Biscay, is still a matter of debate (e.g., *Barnett-Moore et al*., 2016). Currently, no clear consensus exists on the evolution of extensional processes and the development of rift-related basins along the Iberian/European plate boundary.

Left-lateral movements of Iberia relative to Europe have been interpreted to drive the development of a transtensional corridor and an intracontinental rift dissecting Iberia from Late

Jurassic to Early Cretaceous (e.g., *Arche and López-Gómez*, 1996; *Jammes et al.*, 2010b; *Tugend et al.*, 2014). Narrow and deep depocentres of different age developed during this period. Currently, following the NW-SE trend of the major Ventaniella Fault towards the south-east, it is possible to identify (figure 12): the Cabuérniga Basin and the Polientes Basin within the Basque-Cantabrian Zone; the Cameros Basin, the Central and South Iberian Basins and the Maestrazgo Basin as part of the Iberian Rift System, located at present within the Iberian Chain; the Columbrets Basin offshore, at the Eastern Iberian margin. Towards the east, they include the offshore Parentis Basin, and the Arzaq and the Organyà basins, located at present within the western and central Pyrenees. Strong controversies about the structure and kinematic evolution of all these basins prevail (e.g., *Espina*, 1997; *Salas et al.*, 2001; *Vergés and García-Senz*, 2001; *Tavani et al.*, 2018; *Aurell et al.*, 2019; *Martín-Chivelet et al.*, 2019). They might be developed within a diffuse and segmented transtensional corridor accommodating sinistral movements of Iberia relative to Europe, which led to the formation of lozenge shaped pull-apart basins.

Extreme crustal thinning and mantle exhumation have been well-documented from Aptian to Cenomanian in north Iberia (e.g., *Jammes et al.*, 2009; *Roca et al.*, 2011; *Masini et al.*, 2014; *Pedrera et al.*, 2017; *Quintana et al.*, 2015; *Tugend et al.*, 2015; *Cadenas et al.*, 2018; *DeFelipe et al.*, 2019; *García-Senz et al.*, 2019; *Saspiturry et al.*, 2019; *Lescoutre & Manatschal*, 2020). North-dipping extensional detachment faults led to the development of the Biscay rift system (this study), the Basque-Cantabrian Basin (e.g., *Quintana et al.*, 2015; *Pedrera et al.*, 2017; *Tavani et al.*, 2018; *DeFelipe et* al., 2019; *García-Senz et al.*, 2019) and the Mauleón Basin (e.g., *Jammes et al.*, 2009; *Masini et al.*, 2014; *Saspiturry et al.*, 2019; *Lescoutre & Manatschal*, 2020). The link and the spatio-temporal evolution of these hyperextended systems is still unresolved. Based on the widening of the Llanes domain towards the east, we suggest a linkage between this domain and the Basque-Cantabrian Basin.

6.5) Compressional reactivation of the North Iberian multi-stage rift

The inherited, complex rift template influenced the compressional reactivation, and resulted in an amplification of the inherited margin segmentation, controlling the present-day architecture. Each rift system responded differently to compression, accommodating distinctive types and amount of deformation (figures 3c, 4c, 5c, 6c, and 7c).

The *Gijón-Ribadesella System* was mildly inverted (figure 3c). Triassic evaporites played a major role in localising deformation (*Cadenas & Fernández-Viejo,* 2017; *Zamora et al.*, 2017). The squeezing of diapirs and the formation of halokynesis-related structures focused the compression and controlled the shape of the Upper Eocene to Early Miocene syn-orogenic units, with the Triassic evaporites acting as a decoupling level.

The pull-apart *Asturian Basin* was slightly reactivated (figure 4c). Reactivation of the F1, F2, Ayalga and Xana faults, and the development of minor reverse faults and related anticlines, focused the reactivation. This led to the uplift and erosion of the Upper Cretaceous to Eocene post-kinematic units (figures 4c, 6c and 7c). The steep, planar and high-angle F1 and F2 strike-slip faults accommodated minor deformation during the reactivation, leading to the formation of south-directed and north-directed splay reverse faults (figure 4c). The vergence of reverse faults changes from south- to north-directed at the main depocentre. Considering a Santonian onset of the Alpine compression (e.g., *Teixell et al.*, 2018 and references therein) and the end of major transtension in the Hauterivian (see section 6.3.3), the Asturian Basin had 33 Ma to thermally equilibrate. Such a localised, deep and narrow basin, underlain by cold and strong mantle, may indeed be difficult to invert.

The *Biscay System* (e.g., Biscay/Le Danois and Llanes domains) accommodated distinctively most of the reactivation (figures 3c, 4c, and 5c). The hyperthinned and exhumed mantle domains (e.g., hyperextended domains) focused the deformation, as demonstrated for the reactivation of many Alpine Tethys margins (figure 9a, b and c) (e.g., *Mohn et al.*, 2014; *Tugend et al.*, 2014). South-dipping thrusts accommodated the southward underthrusting of highly thinned crust and

exhumed mantle, leading to the development of an overlying accretionary wedge (figures 3c, 4c, and 5c). These thrusts truncated the Biscay and the Llanes detachment systems (e.g., the Biscay Detachment Surface, figure 4c) and decoupled on top of the mantle. We interpret that these thrusts decoupled into exhumed and serpentinized mantle and we speculate that the refraction Moho might correspond to a serpentinization front. Within the hyperthinned and the exhumed mantle domain, minor reactivation of extensional detachment surfaces as thrusts and backthrusts also occurred (figures 3c, 4c, and 5c). The limit between the Le Danois and the Llanes detachment systems was also reactivated (e.g., Lastres Thrust-LT- in figure 9f). The boundary between the exhumed mantle domain and the hyperthinned domain was reactivated across the Biscay and Llanes domains (figure 9a, b, and c), leading to the southward underthrusting of exhumed mantle (e.g., Biscay Thrust-2 in the Biscay domain, in figures 3c and 4c, and Torrelavega Thrust in figure 5c). This reveals that it corresponds to the weakest boundary within the margin, which is deformation-prone,, as it has been proposed in the southern North Atlantic (*Péron-Pinvidic et al.*, 2008) and within the North Atlantic (*Lundin and Doré*, 2011; *Doré and Lundin*, 2015). The boundary between the necking and the hyperthinned domains was also reactivated at some longitudes within the Biscay domain (figure 9b), leading to further underthrusting of highly thinned crust towards the south (e.g., the Le Danois Thrust in figure 4c). This reveals that this corresponds to the second boundary that is deformation-prone.. *Ramos et al.,* (2017) described as well reactivation of this limit in the West Iberian margin. The emplacement of the Le Danois Thrust led to the overthrusting of the Le Danois crustal block (figure 9b). We interpret this block as a passively uplifted and rotated necking zone. On the Llanes system, however, we suggest that the necking zone acted as a local buttress (figure 9c), as reported in Alpine Tethys margins (*Mohn et al*., 2014). Within the proximal and necking domains, the brittle/ductile transition acted as a decoupling level of south-dipping thrusts.

The distribution of compression within the so-called Santander Transfer Zone (*Roca et al*., 2011) exemplifies how the hyperextended domains became the locus of reactivation. Within this

area, we interpret a widening of the Llanes hyperextended domain, which includes highly thinned crust and, locally, exhumed mantle. Underthrusting of exhumed mantle occurred within this area just until the outer limit of the necking zone (figure 5c). Thus, we suggest that during the Alpine orogeny the so called Santander Transfer Zone represented an area of crustal accretion, focusing widely distributed compressional reactivation. The presence of highly thinned crust enabled the development of north-verging thrusts decoupled into serpentinized mantle further to the south and to the north, leading to the jump of the Biscay deformation front.

7) Conclusions

In this work, we show that the architecture of the central North Iberian margin results from multi-stage rather than poly-phase rifting. The margin includes different rift systems, which developed during out of sequence rift events, with different kinematic frameworks and time spans. Each rift system is depicted by an overall crustal structure, basin architecture, bounding structures, and age of syn-kinematic sequences. The spatial distribution and overprint of the three rift systems resulted in a complex 3D margin template. This conditioned the late Alpine orogeny that gave place to the mountain ranges in the north Iberian Peninsula and the accretionary wedge within the Biscay abyssal plain. The results of this study enables us to draw the following conclusions:

1) This work addresses the problem of multi-stage rifting for the first time and documents how multiple rift events result in complex 3D margin architectures.

2) We map and describe distinctive rift-related basins, bounding structures, and crustal domains. High-angle normal faults accommodate diffuse crustal stretching and minor thinning, resulting in the formation of half-graben-type basins. Strike-slip faults lead to high degrees of punctual crustal thinning, involving the development of narrow and laterally confined pull-apart basins.

Extensional detachment faults accommodate necking, extreme crustal thinning and mantle exhumation, leading to the formation of wide hyperextended domains.

3) This tectono-stratigraphic analysis enables to identify a diffuse and widespread rift system of Triassic age, a confined Late Jurassic to Barremian left-lateral transtensional rift system, and a wide Aptian to Cenomanian hyperextended rift system.

4) Strain partitioning during each rift event conditioned its architecture. Inherited rift templates guided subsequent rift events and hence the architecture and overlap of successive rift systems and the final 3D rift template.

5) The inherited rift template conditioned the subsequent margin reactivation. Each rift system accommodates distinctive compressional deformation. Diapirism and halokynesis-related processes tend to focus the compression within the classical half-graben basins. Pull-apart basins are preserved as slightly inverted rift basins, while the hyperextended system focus the compression distinctively. The exhumed mantle and the hyperthinned domains are the locus of deformation, while the necking zone acts as a local buffer or is passively uplifted, tilted and eroded.

6) The interplay of the Alpine compression with the three Mesozoic rift systems amplified the inherited margin segmentation, explaining the ample structural variability observed in the present-day crustal structure.

7) Overprinted multi-stage rift systems can lead to flawed plate kinematic restorations whenever only the final template is considered. The characterisation of the structure and overlap of distinctive rift systems is the keystone to constrain present-day kinematic templates in order to perform accurate plate deformable models on conjugate rifted margins.

The study of the structure and the tectonic evolution of multi-stage rift systems will provide key insights on future research, not only to decipher the spatial and temporal evolution of divergent plate boundaries and the formation of major rift basins, but also to unravel subsequent margin reactivation leading to the uplift o mountain belts. Moreover, the study of multi-stage rift

systems will have major implications on exploration of natural resources. This study shows that these systems include rift-type basins with different pre-/syn- and post-kinematic sedimentary covers and bounding structures, which develop during variable tectono-thermal evolutions.

Acknowledgements

The authors declare that they have no known competing financial interest or personal relationships that could have appeared to influence the work reported in this paper.

No conflict of interest declared

P. Cadenas and G. Manatschal were supported by the ORCLEN Project, a partnership between TOTAL, the INSU-CNRS, and the BRGM. The data have been purchased through the Project MARCAS: CTM2009-11522 of the Ministry of Economy and Competitiveness of Spain. The CS01 2-D seismic data and the boreholes was available through the ATH (https://geoportal.minetur.gob.es/ATHv2/public/). Data interpretation was carried out using Kingdom and Petrel E&P softwares, which were provided by IHS and Schlumberger, respectively, as part of educational programmes. Maps were produced with ArcGIS-ESRI software. P. Cadenas acknowledges the University of Oviedo for providing the data, a workspace, and access to interpretation softwares during short visits. The authors greatly appreciate the valuable and constructive comments, suggestions and discussions that helped to improve the quality of the manuscript provided by Anthony Doré, Gonzalo Zamora, and an anonymous reviewer. The authors thank Rodolphe Lescoutre, Jordi Miró, Josep Anton Muñoz and Luis Quintana for field trips and geological discussions in the Basque-Cantabrian Zone, the western Pyrenees and the Asturian coast, and acknowledge the Orogen Community for discussions during project meetings.

References

Ábalos, B., 2016. Geological map of the Basque-Cantabrian Basin and a new tectonic interpretation of the Basque Arc. International Journal of Earth Sciences 105, 2327-2354. https://doi.org/10.1007/s005331-016-1291-6.

Álvarez-Marrón, J., Pérez-Estaún, A., Dañobeitia, J. J., Pulgar, J. A., Martínez-Catalán, J. R., Marcos, A., Bastida, F., Ayarza Arribas, P., Aller, J., Gallart, J., González-Lodeiro, F., Banda, E., Comas, M.C., Córdoba, D., 1996. Seismic Structure of the northern continental margin of Spain from ESCIN Deep seismic profiles. Tectonophysics 264, 153–174.

Álvarez-Marrón, J., Rubio, E., Torné, M., 1997. Subduction-related structures in the North Iberian margin, Journal of Geophysical Research 102, 22, 497-22,511.

Alves, T.M, Moita, C., Cunha, T., Ullnaess, M., Myklebust, R., Monteiro, J.H., Manuppella, G., 2009. Diachronous evolution of Late Jurassic-Cretaceous continental rifting in the northeast Atlantic (West Iberian margin), Tectonics 28. https://doi.org/10.1029/2008TC002337.

Arche A, López-Gómez, J., 1996. Origin of the Permian–Triassic Iberian Basin, central-eastern Spain. Tectonophysics 266, 443–464.

Aurell, M., Fregenal-Martínez, M., Bádenas, B., Muñoz-García, M.B., Élez, J., Meléndez, N., de Santisteban, C., 2019. Middle Jurassic-Early Cretaceous tectono-sedimentary evolution of the southwestern Iberian Basin (central Spain): Major palaeogeographical changes in the geotectonic framework of the Western Tethys. Earth Sciences Reviews 199. https://doi.org/10.1016/j.earscirev.102983.

Barnett-Moore, N., Hosseinpour, M., Maus, S., 2016. Assessing discrepancies between previous plate kinematic models of Mesozoic Iberia and their constraints. Tectonics 35, 1843–1862. https://doi.org/10.1002/2015TC004019.

Bell, R.E., Jackson, C. A.L., Whipp, P. S., Clements, B. 2014. Strain migration during multiphase extension: Observations from the northern North Sea. Tectonics 33. https://doi.org/10.1002/2014TC003551.

Bertotti, G., Picotti, V., Bernoulli, D., Castellarin, A. From rifting to drifting: tectonic evolulution of the South-Alpine upper crust from the Triassic to the Early Cretaceous. Sedimentary Geology 86,53-76.

Boillot, G., Dupeuble, P. A., Malod, J., 1979. Subduction and Tectonics on the continental margin off northern Spain. Marine Geology 32, 53–70.

Bois, C., Gariel, O., Lefort, J. P., Rolet, J., Brunet, M. F., Masse, P., Olivet, J. L., 1997. Geologic contribution of the Bay of Biscay deep seismic survey: Summary of the main scientific results, a discussion of the open questions and suggestions for further investigation. Mémoires de la Société Géologique de France 171, 193–209.

Cadenas, P., Fernández-Viejo, G., 2017. The Asturian Basin within the North Iberian margin (Bay of Biscay): Seismic characterization of its geometry and its Mesozoic and Cenozoic cover. Basin Research 29, 521–541. https://doi.org/10.1111/bre.12167

Cadenas, P., Fernández-Viejo, G., Pulgar, J.A., Tugend, J., Manatschal, G., Minshull, T.A., 2018. Constraints imposed by rift inheritance on the compressional reactivation of a hyperextended margin: Mapping rift domains in the North Iberian margin and in the Cantabrian Mountains. Tectonics 37. https://doi.org/10.002/2016TC004354.

Capdevila, R., Boillot, B, Lepvrier, C., Malod, J.A., Mascle, G., 1980. Metamorphic and plutonic rocks from the Le Danois Bank (North Iberian Margin). Comptes Rendus Hebdomadaires des Seances de L´Academie Des Sciences 291,317-320.

Chenin, P., Manatschal, G., Picazo, S., Müntener, O., Karner, G., Johnson, C., Ulrich, M., (2017). Influence of the architecture of magma-poor hyperextended rifted margins on orogens produced by the closure of narrow versus wide oceans. Geosphere 13, 559-576. http://doi.org/10.1130/GES01363.1.

Cowie, P. A., Underhill, J.R., Behn, M.D., Lin, J., Gill, C.E., 2005. Spatio-temporal evolution of strain accumulation derived from multi-scale observations of Late Jurassic rifting in the northern North Sea:

A critical test of models for lithospheric extension, Earth and Planetary Sciences 234, 401–419. http://doi.org/10.1016/j.epsl.2005.01.039.

DeFelipe, I., Pedreira, D., Pulgar, J.A., Beek, P.A., Bernet, M., Pik, R., 2019. Unraveling the Mesozoic and Cenozoic Tectonothermal Evolution of the Eastern Basque-Cantabrian Zone-Western Pyrenees by Low Temperature Thermochronology. Tectonics 38. http://doi.org/10.1029/2019TC005532.

Déregnaucourt, D., Boillot, G., 1982. New structural map of the Bay of Biscay. In Comptes Rendus De L´Academie Des Sciences 294, 219–222.

Doré, T., Lundin, E., 2015. Hyperextended continental margins-Knowns and unknowns. Geology 43, 95-96.http://doi.org/10.1130/focus012015.1.

Espina, R., (1997). La estructura y evolución tectonoestratigráfica del borde occidental de la Cuenca Vasco-Cantábrica (Cordillera Cantábrica, NO de España). PhD thesis, Oviedo University.

Etheve, N., Mohn, G., Frizon de Lamotte, D., Roca, E., Tugend, J., Gómez-Romeu, J., 2018. Extreme Mesozoic Crustal Thinning in the Eastern Iberia Margin: The Example of the Columbrets Basin (Valencia Trough), Tectonics 37. https://doi.org/10.1002/2017TC004613.

Fernández-Lozano, J., Gutiérrez-Alonso, G., Willingshofer, E., Sokoutis, D., de Vicente, G., Cloetingh, S., 2019. Shaping of intraplate mountain patters: The orocline legacy in Alpine Iberia. Lithosphere 11, 708-721. https://doi.org/10.1130/L1079.1.

Fernández-Viejo, G., Gallart, J., Pulgar, J. A., Gallastegui, J., Dañobeitia, J. J., Córdoba, D., 1998. Crustal transition between continental and oceanic domains along the North Iberian margin from wide angle seismic and gravity data. Geophysical Research Letters 25, 4249–4252. https://doi.org/10.1029/1998GL900149.

Fernández-Viejo, G., Gallastegui, J., Pulgar, J. A., Gallart, J., 2011. The MARCONI reflection seismic data: A view into the eastern part of the Bay of Biscay. Tectonophysics 508, 34–41. https://doi.org/10.1016/j.tecto.2010.06.020.

Fernández-Viejo, G., Pulgar, J. A., Gallastegui, J., Quintana, L., 2012. The fossil accretionary wedge of the Bay of Biscay: Critical wedge analysis on depth-migrated seismic sections and geodynamical implications. Journal of Geology 120, 315–331. https://doi.org/10.1086/664789.

Ferrer, O., Roca, E., Benjumea, B., Muñoz, J. A., Ellouz, N., MARCONI Team, 2008. The deep seismic reflection MARCONI-3 profile: Role of extensional Mesozoic structure during the Pyrenean contractional deformation at the eastern part of the Bay of Biscay. Marine and Petroleum Geology 25, 714–730.https://doi.org/10.1016/j.marpetgeo.206.002

Fügenschuh, B., Froitzheim, N., Capdevila, R., Boillot, G., 2003. Offshore granulites from the Bay of Biscay margins: fission tracks constrain a Proterozoic to Tertiary thermal history. Terra Nova 15, 337-342. https://doi.org/10.1046/j.1365.3121.2003.00502.

Gallastegui, J., Pulgar, J. A., Gallart, J., 2002. Initiation of an active margin at the North Iberian continent-ocean transition. Tectonics 21,1033. https://doi.org/10.1029/2001TC901046.

García-Mondéjar, J., 1996. Plate reconstruction of the Bay of Biscay. Geology 24, 635–638.

García-Senz, J., Pedrera, A., Ayala, C., Ruiz-Constán, A., Robador, A., Rodríguez-Fernández, L.R. 2019. Inversion of the North Iberian hyperextended margin: the role of exhumed mantle indentation during continental collision. Geological Society Special Publications, 490. https: //doi.org/10.1144/SP490-

Gouiza, M., Hall, J., Welford, J.K., 2017. Tectono-stratigraphic evolution and crustal architecture of the Orphan Basin during North Atlantic rifting. International Journal Earth Sciences 106, 917-937. https:// doi.org/10.1007/s00531-016-1341-0.

Gutiérrez-Claverol, M., Gallastegui, J., 2002. Prospección de hidrocarburos en la plataforma continental de Asturias. Trabajos de Geologia 23, 21–34.

Jammes, S., Manatschal, G., Lavier, L., Masini, E., 2009. Tectonosedimentary evolution related to extreme crustal thinning ahead of propagating ocean: Example of the western Pyrenees. Tectonics 28. https://doi.org/10.1029/2008TC002406.

Jammes, S., Manatschal, G., Lavier, L., 2010a. Interaction between prerift salt and detachment faulting in hyperextended rift systems: The example of the Parentis and Mauleón basins (Bay of Biscay and western Pyrenees), AAPG Bulletin 94, 957-9725. https://doi.org/10.1306/12090909116.

Jammes, S., Tiberi, C., Manatschal, G., 2010b. 3D architecture of a complex transcurrent rift system: The example of the Bay of Biscay-Western Pyrenees. Tectonophysics 489, 210–226. https://doi.org/10.1016/j.tecto.2010.04.023.

Laughton, A.S., *et al.*, (1971), Site 118. In: A.S. Laughton, A.S., et al. (Eds), Initial Reports of the Deep Sea Drilling Project Covering Leg 12 of the Cruises of the Drilling Vessel Glomar Challenger, Boston, Massachusetts to Lisbon, Portugal, 12, 673-751.

Lavier, L. L., Manatschal, G., 2006. A mechanism to thin the continental lithosphere at magma-poor margins. Nature 440, 324-328. https://doi.org/10.1038/nature04608.

Lepvrier, C., Martínez-García, E., 1990. Fault development and stress evolution of the post-Hercynian Asturian Basin (Asturias and Cantabria, northwestern Spain). Tectonophysics 184, 345–356.

Lister, G., 1986. Detachment faulting and the evolution of passive continental margins. Geology 14, 246–250.

López-Gómez, J.L., Martín-González, F., Heredia, N., de la Horra, R., Barrenechea, J.F., Cadenas, P., Juncal, M., Diez, J.B., Borruel-Abadía, V., Pedreira, D., García-Sansegundo, J., Farias, P., Galé, C., Lago, M., Ubide, T., Fernández-Viejo, G., Gand, G., 2019. New lithostratigraphy for the Cantabrian Mountains: A common tectono-stratigraphic evolution for the onset of the Alpine cycle in the W Pyrenean realm, N Spain. Earth Sciences Reviews 188, 249-271. https://doi.org/10.1016/j.earscirev.2018.11.008.

Lescoutre, R., 2019. Formation and reactivation of the Pyrenean-Cantabrian rift system: inheritance, segmentation and thermal evolution. PhD Thesis. Strasbourg University.

Lescoutre, R. and Manatschal, G. (in press). Role of rift inheritance and segmentation for orogenic evolution: example from the Pyrenean-Cantabrian system. Bulletin de la Société Géologique de France

Lymer, G., Cresswel, D.J.F., Reston, T.J., Bull, J.M., Sawyer, D.S., Morgan, J.K., Stevenson, C., Causer, A., Minshull, T.A., Shillington, D.J., 2019. 3D development of detachment faulting during continental breakup. Earth and Planetary Sciences Letters 515, 90-99. https://doi.org/ 10.1016/j.epsl.2019.03.018.

Lundin, E. R., Doré, A. G., 2011. Hyperextension, serpentinization, and weakening: A new paradigm for rifted margin compressional deformation. Geology 39, 347–350. https://doi.org/10.1130/G31499.1.

Malod, J., Boillot, G., Capdevila, R., Dupeuble, P.A., Lepvrier, C., Mascle, G., Taugourdeu-Lantz, J., 1982. Subduction and tectonics on the continental margin off northern Spain; observations with the submersible Cyana. In: Legett, J.K., (Ed), Trench-Fore Arc Geology, Geological Society of London Special Publications 10, 309-315.

Mann, P., 2007. Global catalogue, classification and tectonic origin of restraining-and releasing bends on active and ancient strike-slip fault systems. In: Cunningham, W.D., Mann, P. (Eds), Tectonics of Strike-Slip Restraining and Releasing Bends. Geological Society of London Special Publications 290, 13-142.

Martín-Chivelet, J., López-Gómez, J., Aguado, R., Arias, C., Arribas, J., Arribas, M.E., Aurell, M., Bádenas, B., Benito, M.I., Bover-Arnal, T., Casas-Sainz, A., Castro, J.M., Coruña, F., de Gea, G.A., Fornós, J.J., Fregenal-Martínez, M., García-Senz, J., Garófano, D., Gelabert, B., Giménez, J., González-Acebrón, L., Guimerà, J., Liesa, C.L., Mas, R., Meléndez, N., Molina, J.M., Muñoz, J.A., Navarrete, R., Nebot, M., Nieto, L.M., Omodeo-Salé, S., Pedrera, A., Peropadre, C., Quijada, I.E., Quijano, M.L., Reolid, M., Robador, A., Rodríguez-López, J.P., Rodríguez-Perea, A., Rosales, I., Ruiz-Ortíz, P.A., Sàbat, F., Salas, R., Soria, A.R., Suárez-González, P., and Vilas, L. (2019). The Late

Jurassic-Early Cretaceous Rifting. In: Quesada, C., Oliveira, J.T., (Eds.), The Geology of Iberia: A Geodynamic Approach, Regional Geology Reviews. https://doi.org/10.1007/978-3-030-11295-0_5.

Masini, E., Manatschal, G., Tugend, J., Mohn, G., 2014. The tectono-sedimentary evolution of a hyper-extended rift basin: The example of the Arzacq-Mauléon rift system (Western Pyrenees, SW France), International Journal of Earth Sciences 103, 1569-1596. https://doi.org/10.1007/s00531-014-1023-8.

McKenzie, D.P., 1978. Some remarks on the development of sedimentary basins. Earth and Planetary Science Letters 40, 20-32.

Montadert, L., Damotte, B., Delteil, J.R., Valery, P., Winnock, E., 1971. Structure géologique de la marge continentale septentrionale du Golfe de Gascogne, In: Debysier, J., Le Pichon, X., Montadert, M., (Eds), Historie structurale du Golfe de Gascogne V, V. II 2-III.2-20.

Mohn, G., Manatschal, G., Beltrando, M., Haupert, I., 2014. The role of rift-inherited hyperextension in Alpine-type orogens. Terra Nova 26, 347–353 https://doi.org/10.1111/ter.12104.

Morley, C.K., Haranya, C., Phoosongsee, W., Pongwapee, S., Kornsawan, A., and Wonganan, N., 2004. Activation of rift oblique and rift parallel pre-existing fabrics during extension and their effect on deformation style: examples from the rifts of Thailand. Journal of Structural Geology 26, 1803-1829. https://doi.org/10.1016/j.jsg.2004.02.014.

Murillas, J., Mougenot, D., Boillot, G., Comas, M.C., Banda, E., and Mauffret, A., 1990. Structure and evolution of the Galicia Interior Basin (Atlantic western Iberian continental margin). Tectonophysics 184, 297-319.

Nirrengarten, M., Manatschal, G., Tugend. J., Kusznir, N., Sauter, D., 2018. Kinematic evolution of the Southern North Atlantic: Implications for the Formation of Hyperextended Rift Systems. Tectonics 37, 89-118. https://doi.org/10.1002/2017TC004495.

Norton, I., Carruthers, D.T., Hudec, M.R., 2016. Rift to drift transition in the South Atlantic salt basins: A new flavor of oceanic crust. Geology 44, 55-58. https://doi.org/10.1130/G37265.1.

Peace, A.L., Welford, J.K., Ball, P.J., Nirrengarten, M., 2019. Deformable plate tectonic models of the southern North Atlantic. Journal of Geodynamics 128, 11-37. https://doi.org/ 10.1016/j.jog.2019.05.005.

Peace, A., McCaffey, K., Imber, J., van Hunen, J., Hobbs, R., Wilson, R., 2018. The role of pre-existing structures during rifting, continental breakup and transform system development, offshore West Greenland. Basin Research 30, 373-394.https://doi.org/10.1111/bre.12257.

Pedreira, D., Pulgar, J.A., Gallart, J., Díaz, J., 2003. Seismic evidence of Alpine crustal thickening and wedging from the western Pyrenees to the Cantabrian Mountains (north Iberia), Journal of Geophysical Research, 108, B42204. https://doi.org/10.1029/2001JB001667.

Pedrera, A., García-Senz, J., Ayala, C., Ruiz-Constán, A., Rodríguez-Fernández, L.R., Robador, A., González-Menéndez, L., 2017. Reconstruction of the Exhumed Mantle Across the North Iberian margin by crustal-scale 3D gravity inversion and geological cross-section: mantle along the Basque-Cantabrian Basin. Tectonics 36, 3155-3177. https://doi.org/10.1002/2017TC004716.

Pereira, R., Alves, T.M., 2012. Tectono-stratigraphic signature of multiphased rifting on divergent margins (deep-offshore southwest Iberia, North Atlantic). Tectonics 31. https://doi.org/10.1029/2011TC003001.

Pérez-Gussinyé, M., Ranero, C. R., Reston, T. J., Sawyer, D., 2003. Mechanisms of extension at non-volcanic margins. Evidence from the Galicia interior basin, west of Iberia. Journal of Geophysical Research 108, 2245. https://doi.org/10.1029/2001JB000901.

Péron-Pinvidic, G., Manatschal, G., 2009. The final rifting evolution at deep magma-poor passive margins from Iberia-Newfoundland: a new point of view. International Journal of Earth Sciences 98, 1581-1597. https://doi.org/10.1007/s00531-008-0337-9.

Péron-Pinvidic, G., Manatschal, G., Osmundsen, P. T., 2013. Structural comparison of archetypal Atlantic rifted margins: A review of observations and concepts. Marine and Petroleum Geology 43, 21–47. https://doi.org/10.1016/j.marpetgeo.2013.02.002.

Péron-Pinvidic, G., Manatschal, G., Dean, S.M., Minshull, T.A., 2008. Compressional structures on the West Iberia rifted margin: controls on their distribution. In: Johnson, H., Doré, A.G., Gatlift, R.W., Holdworth, R., Lundin, E.R., Ritchie, J.D. (Eds), The Nature and Origin of Compression in Passive Margins 306, 169-183, Geological Society of London Special Publications. https://doi.org/10.1144/SP306.8.

Phillips, T.B., Fazlikhani, H., Gawthorpe, R.L., Fossen, H., Jackson, C.A., Bell, R.E., Feleide, J.I., Rotevatn, A., 2019. The influence of structural inheritance and multiphase extension on rift development, the northern North Sea. Tectonics 38. https://doi.org/10.1029/2019TC005756.

Pieren, A. P., Areces, J. L., Toraño, J., Martínez-García, E., 1985. Estratigrafía y estructura de los materiales permotriásicos del sector Gijón-La Collada (Asturias). Cuadernos de Geología Ibérica 19, 309–335.

Quintana, L. (2012). Extensión e inversión tectónica en el sector central de la Región Vasco-Cantábrica. PhD Thesis. Oviedo University.

Quintana, L., Pulgar, J.A., Alonso, J.L., 2015. Displacement transfer from borders to interior of a plate: A crustal transect of Iberia. Tectonophysics 663, 378-398. https://doi.org/10.1016/j.tecto.2015.08.046.

Ramos, A., Fernández, O., Tomé, M., Sánchez de la Muela, A., Muñoz, J.A., Terrinha, P., Manatschal, G., Salas, M. C. (2017). Crustal structure of the SW Iberian passive margin: The westernmost remnant of the Ligurian Tethys?. Tetonophysics 705, 42-62. https://doi.org/10.1016/j.tecto.2017.03.012.

Ranero, C.R., Pérez-Gussinyé, M., 2010. Sequential faulting explains the asymmetry and extension discrepancy of conjugate margins. Nature 468, 294-299.

Rat, P., 1988. The Basque-Cantabrian Basin between the Iberian and European plates. Some facts but still many problems, Revista de la Sociedad Geológica de España, 1.327-347.

Reemst, P., Cloetingh, S., 2000. Polyphase rift evolution of the Vøring margin (mid-Norway): Constraints from forward tectonostratigraphic modeling. Tectonics 19(2), 225-240. https://doi.org/10.1029/1999TC900025.

Reston, T.J., 2005. Polyphase faulting during the development of the west Galicia rifted margin. Earth and Planetary Sciences Letters 237, 561-576. https://doi.org/10.1016/j.epsl.2005.06.019.

Reston, T.J., Gaw, V., Pennell, J., Klaschen, D., Stubenrauch, A., Walker, I., 2004. Extreme crustal thinning in the south Porcupine Basin and the nature of the Porcupine Median High: implications for the formation of non-volcanic rifted margins. Journal of the Geological Society 161,783‑798.

Riaza, C., 1996. Inversión estructural en la cuenca mesozoica del off-shore asturiano. Revisión de un modelo exploratorio. Geogaceta 20, 169–171.

Ribes, C., Petri, B., Ghienne, J.F., Manatschal, G., Galster, F., Karner, G.D., Figueredo, P.H., Johnson, C.A., Karpoff, A.M., 2019. Tectono-sedimentary evolution of a fossil ocean-continent transition. Tasna nappe, central Alps, (SE Switzerland). Geological Society of American Bulletin.

Roca, E., Muñoz, J. A., Ferrer, O., Ellouz, N., 2011. The role of the Bay of Biscay Mesozoic extensional structure in the configuration of the Pyrenean orogen: Constraints from the MARCONI deep seismic reflection survey. Tectonics, 30. https://doi.org/10.1029/ 2010TC002735.

Roest, W. R., and Srivastava, S. P., 1991. Kinematics of the plate boundaries between Eurasia, Iberia and Africa in the North-Atlantic from the Late Cretaceous to the present. Geology 19, 613–616. https://doi.org/10.1130/0091-7613.

Roma, M., Ferrer, O., Roca, E., Pla, O., Escosa, F.O., Butillé, M., 2018. Formation and inversion of salt-detached ramp-syncline basins. Results from analog modeling and application to the Columbrets Basin (Western Mediterranean). Tectonophysics 745, 214-228.https://doi.org/10.1016/j-tecto.2018.08.012.

Ruiz, M. 2007. Caracterització estructural i sismotectònica de la litosfera en el domini Pirenaico-Cantàbric a partir de mètodes de sísmica activa i passiva. PhD Thesis. University of Barcelona.

Ruiz, M., Díaz, J., Pedreira, D., Gallart, J., Pulgar, J.A., 2017. Crustal structure of the North Iberian continental margin from seismic refraction/wide-angle reflection profiles. Tectonophysics 717, 65-82. https:// doi.org/10.1016/j.tecto.2017.07.008.

Salas R, Guimerà J, Mas R, Martín-Closas C, Meléndez A, Alonso, A., 2001. Evolution of the Mesozoic Central Iberian Rift System and its Cenozoic inversión (Iberian Chain). In: Ziegler, P.A., Cavazza, W., Robertson, A.H.F., Crasquin-Soleau, S., (Eds), Peri-Tethyan Rift/Wrench Basins and Passive Margins. Mémoires du Muséum National d' Histoire Naturelle 186,145–185.

Sandoval, L., Welford, J.K., MacMahon, H., Peace, A.L., 2019. Determining continuous basins across conjugate margins: The East Orphan, Porcupine, and Galicia Interior basins of the southern North Atlantic Ocean, Marine and Petroleum Geology 110, 138-161. https:// doi.org/10.1016/j.marpetgeo.2019.06.047.

Santantonio, M., Carminati, E., 2011. Jurassic rifting evolution of the Apennines and Southern Alps (Italy): Parallels and differences. Geological Society of America Bulletin 123, 498-484, https://doi.org/10.1130/B30104.1.

Saspiturry, N., Razin, P., Baudin, T. Serrano, O., Issautier, B., Lasseur, E., Allanic, C., Thinon, I., Leleu, S. 2019. Symmetry vs asymmetry of a hyperthinned rift: Example of the Mauleón Basin (Western Pyrenees). Marine and Petroleum Geology, 104, 86-105. https://doi.org/10.1016/j.marpetgeo.2019.03.031.

Schiffer, C., Dore, A.G., Foulger, G.R., Franke, D., Geoffroy, L., Gernigon, L., Holdsworth, B., Kusznir, N., Lundin, E., McCaffey, K., Peace, A.L., Petersen, K.D., f, T.B., Stephenson, R., Stoker, M.S., and Welford, J.K., 2019. Structural inheritance in the North Atlantic, Earth Sciences Review. https://doi.org/10.1016/j.earscirev.102975.

Sibuet, J. C., Collette, B. J., 1991. Triple junctions of Bay of Biscay and North Atlantic: New constraints on the kinematics evolution. Geology 19, 522–525.

Sibuet, J. C., Srivastava, S. P., Spakman, W., 2004. Pyrenean orogeny and plate kinematics. Journal of Geophysical Research 109, B08104. https://doi.org/10.1029/2003JB002514.

Smith, J., Brun, J.P., Cloething, S., Ben-Avraham, Z. 2008. Pull-apart basin formation and development in narrow transform zones with application to the Dead Sea Basin. Tectonics 27. htpps://doi.org/10.1029/2007TC002119.

Srivastava, S. P., Sibuet, J. C., Cande, S., Roest, W. R., Reid, I. D., 2000. Magnetic evidence for slow seafloor spreading during the formation of the Newfoundland and Iberian margins. Earth and Planetary Science Letters 182, 61–76. https://doi.org/10.1016/S0012-821X (00)0023, 1-4.

Suárez-Rodríguez, A., 1988. Estructura del área de Villaviciosa-Libardón (Asturias, Cordillera Cantábrica). Trabajos de Geologia 17, 87–98.

Sutra, E., Manatschal, G. Mohn, G., Unternehr, P., 2013. Quantification and restoration of extensional deformation along the Western Iberia and Newfoundland rifted margins. Geochemistry, Geophysics, Geosystems 14, 2575–2597. https://doi.org/10.1002/ggge.20135.

Tavani, S., Bertok, C., Granado, P., Piana, F., Salas, R., Vigna, B., Muñoz, J.A., 2018. The Iberia-Eurasia plate boundary east of the Pyrenees. Earth Sciences Review 187, 314-337, https://doi.org/10.1016/j.earscirev.2018.10.008.

Teixell, A., Labaume, P., Ayarza, P., Espurt, N., de Saint Blanquat, M., Lagabrielle, Y., 2018. Crustal structure and evolution of the Pyrenean-Cantabrian belt: A review and new interpretations from recent concepts and data. Tectonophysics 724-725, 146-170. https://doi.org/ 10.1016/j.tecto.2018.01.009.

Thinon, I., Matias, L., Réhault, J. P., Hirn, A., Fidalgo-Gonzalez, L., Avedik, F., 2003. Deep structure of the Armorican Basin (Bay of Biscay): A review of Norgasis seismic reflection and refraction data. Journal of the Geological Society 160, 99–116.

Thinon, I., Réhault, J.P., Fidalgo-González, L., 2002. The syn-rift sedimentary cover of the North Biscay Margin (Bay of Biscay): From new reflection seismic data. Bulletin de la Societé Géologique de France 173, 515–522.

Tugend, J., Manatschal, G., Kusznir, N. J., Masini, E., Mohn, G., Thinon, I., 2014. Formation and deformation of hyperextended rift systems: Insights from rift domain mapping in the Bay of Biscay-Pyrenees. Tectonics 33, 1239–1276. https://doi.org/10.1002/2014TC003529.

Tugend, J., Manatschal, G., Kusznir, N. J., Masini, E., 2015. Characterizing and identifying structural domains at rifted continental margins: application to the Bay of Biscay margins and its Western Pyrenean fossil remnants. In Gibson, G.M. et al. (Eds.), Sedimentary basins and crustal processes at continental margins: from modern hyper-extended margins to deformed ancient analogues. Geological Society of London Special Publication 413, 171–203. https://doi.org/10.1144/SP413.3.

Uzkeda, H., Bulnes, M., Poblet, J., García-Ramos, J. C., Piñuela, L., 2016. Jurassic extension and Cenozoic inversion tectonics in the Asturian Basin, NW Iberian Peninsula: 3D structural model and kinematic evolution. Journal of Structural Geology 90, 157–176.

Valenzuela, M., García-Ramos, J. C., Suárez de Gerdi, C., 1986. The Jurassic sedimentation in Asturias (N Spain). Trabajos de Geologia 16, 121–132.

Vergés, J., García-Senz, J., 2001. Mesozoic evolution and Cainozoic inversion of the Pyrenean Rift. In: Ziegler, P.A., et al. (Eds.), Peri-Tethys Memoir 6: Peri-Tethyan Rift/ Wrench Basins and Passive Margins, Mémoires Museum Histoire Naturelle 186, 187–212.

Vissers, R. L. M., Meijer, P. T., 2012. Mesozoic rotation of Iberia: Subduction in the Pyrenees? Earth-Science Reviews 110, 93–110. https://doi. org/10.1016/j.earscirev.2011.11.001.

Watremez, L., Prada, M., Minshull, T.A., O’ Reilly, B.M., Chen, C., Reston, T.J., Shannon, P.M., Wagner, G., Gaw, V., Klaschen, D., Edwards, R., Lebedev, S., 2016. Deep structure of the Porcupine Basin from wide-angle seismic data. Petroleum Geology Conference Series 8, 199‑209. https://doi.org/10.1144/PGC8.26.

Welford, J.K., Shannon, P.M., O’Reilly, B.M. Hall, J., 2012. Comparison of lithosphere structure across the Orphan Basin–Flemish Cap and Irish Atlantic conjugate continental margins from constrained 3D gravity inversions, Journal of Geological Society of London 169(4), 405–420.

Wernicke, B., 1985. Uniform-sense normal simple shear of the continental lithosphere. Canadian Journal of Earth Sciences 22, 108-125.

Whitmarsh, R.B., Manatschal, G., Minshull, T.A., 2001. Evolution of magma-poor continental margins from rifting to seafloor spreading. Nature 413, 150-154. https://doi.org/ 10.1038/35093085.

Wilson, R.C.L., Manatschal, G., Wise, S., 2001. Rifting along non-volcanic passive margins: stratigraphic and seismic evidence from the Mesozoic successions of the Alps and western Iberia. In: Wilson, R.C.L., R.B. Whitmarsh, Taylor, B., Froitzhem, N. (Eds), Non-Volcanic Rifting of Continental Margins: A Comparison of Evidence from Land and Sea. Geological Society of London Special Publication 187, 429-452.

Zalan, P. V., do Carmo., G., Severino, M., Rigoti, C.A., Magnavita, L.P., Bach de Oliveira, J.A., Roessler Vianna, A., 2011. An Entirely New 3D-View of the Crustal and Mantle Structure of a South Atlantic Passive Margin – Santos, Campos and Espírito Santo Basins, Brazil, In: AAPG Annual Convention and Exhibition.

Zamora, G., Fleming, M., Gallastegui, J., 2017. Salt Tectonics within the offshore Asturian Basin: North Iberian margin, In: Soto, J.I., Flinch, J.F., Tari, G. (Eds.), Permo-Triassic salt provinces of Europe, North Africa and the Atlantic Margins, Chapter16, 358-368.

Ziegler, P. A., Dèzes, P., 2006. Crustal evolution of Western and Central Europe. In Gee, D.G., Stephenson, R.A., (Eds.), European lithosphere dynamics 32, 43–56.

Figure Captions

Figure 1: a) Location of the studied zone in the context of the Bay of Biscay; **AB**: Asturian Basin; **LC**: Lastres canyon; **LDH**: Le Danois High; **LLC**: Llanes canyon; **SC**: Santander canyon; **SP**: Santander Promontory; **TC**: Torrelavega canyon; **b)** Palaeographic rift domains map showing the structure of the Bay of Biscay, the Pyrenean-Basque Cantabrian, and the Iberian rifts before Santonian

(*Tugend et al.*, 2015). **BoB:** Bay of Biscay Rift; **Ib**: Iberian Rift; **Py-BCB**: Basque-Cantabrian Rift; **c)** Present-day rift domains map for north Iberian rift systems. Rift domains in the Pyrenean-Basque-Cantabrian rifts, in the Armorican margin and in the eastern North Iberian margin are from *Tugend et al.* (2015). Rift domains in the central and western North Iberian margin and within the Cantabrian Mountains are from *Cadenas et al.* (2018). The map displays the distribution of the available dataset **AB**: Asturian Basin; **BAW**: Biscay accretionary wedge; **LDH**: Le Danois High; **STZ**: Santander Transfer Zone. Plain. The time scale shows the temporal distribution of the major tectonic events, which occurred within the studied zone; **d)** Detailed location of the CS01 reflection profiles and boreholes used in this study.

Figure 2: Well-log based stratigraphy and interpretation of the main tectonic units along four representative boreholes; **a)** Seismic to well ties. The first column displays the sonic log and the time to depth profile used to constrained the velocity model and introduce the well data within the reflection profiles. The second column shows an overlapped seismic section along the borehole with the interpretation of the main tectonic units on top**; b)** Stratigraphic record and interpretation of the main tectonic units and formation tops along the boreholes; Boreholes MC-H1X, MC-K1, and MC-C4, after *Cadenas and Fernández-Viejo* (2017).

Figure 3: a) Profile CS01-124, running in the central North Iberian margin from south to north. The location of the seismic line and the borehole Asturias-D2 Bis (AST-D2Bis) (projected) is displayed in figure 1c and d; **b)** Ray tracing and interpretation of reflectivity patters. The figure shows the velocity profile and the time-to-depth chart used to introduce borehole Asturias-D2Bis within the seismic profile; **c)** CS01-124 cross-section. **BR-BD**: Break-aways of extensional detachment faults belonging to the Biscay Detachment System (BD). The transparency delineates areas with less seismic and borehole constraints, where the interpretation results from the geological knowledge.

Figure 4: a) Profile CS01-132, running in the central North Iberian margin from south to north. The location of the seismic profile and the boreholes Mar Cantábrico-H1X (MC-H1X) and Mar

Cantábrico-C4 (MC-C4) is displayed in figures 1c and d; **b)** Ray tracing and seismic interpretation of reflectivity patters. The figure shows the velocity profile and the time-to-depth chart used to introduce boreholes Mar Cantábrico-C4 and Mar Cantábrico-H1X within the seismic profile; **c)** CS01-132 cross-section. **BR-LD**: Break-aways of extensional detachment faults belonging to the Le Danois Detachment System (LD). The transparency delineates areas with less seismic and borehole constraints, where the interpretation results from the geological knowledge.

Figure 5: a) Profile CS01-146, running in the central North Iberian margin from south to north. The location of the seismic profile is displayed in figure 1c and d. **b)** Ray tracing and seismic interpretation of reflectivity patters; **c)** CS01-146 cross-section. **BR-LL**: Break-aways of extensional detachment faults belonging to the Llanes Detachment System (LLD). The transparency delineates areas with less seismic and borehole constraints, where the interpretation results from the geological knowledge.

Figure 6: a) Profile CS01-104a, running in the central North Iberian margin from west to east. The location of the seismic line and the borehole Asturias-D2 Bis (AST-D2Bis) is shown in figure 1c and d; **b)** Ray tracing and seismic interpretation of reflectivity patters. The figure displays the time-to-depth column used to introduce the borehole Asturias-D2Bis within the seismic line; **c)** CS01-104a cross-section. The transparency delineates areas with less seismic and borehole constraints, where the interpretation results from the geological knowledge.

Figure 7: a) Profile CS01-104b, running in the central North Iberian margin from west to east. The location of the profile is shown in figure 1c and d; **b)** Ray tracing and seismic interpretation of reflectivity patters; **c)** CS01-104b cross-section. Vertical logs show the interpretation along N-S profiles at the intersection with the CS01-104 line. **LL-1, -2, -3**: intersections of the Llanes Detachment-1, -2 and -3, belonging to the Llanes Detachment System (LLD). The transparency delineates areas with less seismic and borehole constraints, where the interpretation results from the geological knowledge.

Figure 8: **a)**, **b)**, and **c)** Interpretation of the base and the top of the Upper Jurassic to Barremian syn-rift unit 2 and the major extensional and compressional structures along the CS01-124, CS01-132, and CS01-104a cross-sections. The maps in figures d, e, and f show the location of the profiles; **d)** Contour map showing the depth of the base of the Upper Jurassic to Barremian syn-rift unit 2 and the cutting points of the master F1 and F2 strike-slip faults and the Ayalga and Xana dip slip faults, which bound the Asturian Basin; **e)** Contour map displaying thickness variations of the Upper Jurassic to Barremian syn-rift unit 2 and the cutting points of the F1, F2, Ayalga, and Xana faults; **f)** Structural map showing the geometry of the Asturian Basin and the trend of the F1 and F2 master strike-slip faults and the Ayalga and Xana dip-slip normal faults.

Figure 9: **a)**, **b)**, and **c)** Interpretation of the base and the top of the Aptian to Cenomanian syn-rift unit 3 and the major extensional and compressional structures along the CS01-124, CS01-132, and CS01-146 cross-sections. The maps in figures d, e, and f show the location of the profiles. Rift domains are defined on top of the profiles; **d)** Contour map showing the depth of the base of the Aptian to Cenomanian syn-rift unit-3 and the location of the Le Danois (BR-LD), the Biscay (BR-BB), and the Llanes (BR-LL) break-away points and the southernmost and northernmost thrust decoupled in the mantle and in the brittle/ductile transition respectively. **e)** Contour map displaying thickness variations of the Aptian to Cenomanian syn-rift unit-3. The map shows the same structural features displayed in figure d; **f)** Structural map showing the geometry and the extend of the Biscay/Le Danois and the Llanes hyperextended systems, and the trend of the Le Biscay/Le Danois and the Llanes Break-away lineaments, which delimit and bound these domains. **BT:** Biscay Thrust; **BT-2**: Biscay Thrust-2; **LDT**: Le Danois Thrust; **LT**: Lastres Thrust; **LLT**: Llanes Thrust; **TT**: Torrelavega Thrust.

Figure 10: a) Qualitative restoration of the CS01-132 cross-section before the onset of the Alpine convergence (e.g., before Santonian), showing the crustal structure and basin architecture, the age, and the kinematic features of the multi-stage North Iberian rift at 4º30´W. **b)** Structural map showing the present-day distribution, extent and overlap of the Gijón-Ribadesella, the Asturian, and the Biscay rift

systems. **F1 and F2**: master strike-slip faults; **AF**: Ayalga Fault; and **XF**: Xana Fault: dip-slip normal faults. **BR-BD**: Biscay Break-away lineament; **BR-LD**: Le Danois Break-away lineament; **BR-LL**: Llanes Break-away lineament; **c)** Map showing the distribution of rift domains within an idealized poly-phase rift system as described by *Tugend et al*. (2015); **d)** 2D architecture of an idealized poly-phase rift system, based on *Péron-Pinvidic et al.* (2013), *Ribes et al.* (2019), *Sutra et al.* (2013), and *Tugend et al*. (2015).

Figure 11: Formation and tectono-stratigraphic evolution of the Gijón-Ribadesella, the Asturian, and the Biscay rift systems from Triassic to Coniacian. The figure shows the distribution of rift-related sediments and bounding structures, the tectonic activity and the rift-related units, and the time constraints.

Figure 12: Map showing the location of major Mesozoic rift basins, which have been described in north and east Iberia. These basins are preserved at present within the North Iberian margin and the Eastern Iberian margin, and within the Basque-Cantabrian Zone (BCZ), the Pyrenees, and the Iberian Chain onshore. Asturian Basin (**AB**) and Biscay/Le Danois and Llanes systems, from this study. Cabuérniga Basin (**CBB**) and Polientes Basin (**PB**) from *Ábalos* (2016) and *Espina* (1997). Basque-Cantabrian Basin (**BCB**), Mauleón Basin (**MB**), and Arzaq Basin (AZB) from *Masini et al*., 2014 and *Lescoutr*e (2019). Organyà Basin (**OB**) from *Tavani et al.* (2018). Cameros Basin (**CB**), Central Iberian Basins, South Iberian Basins, and Maestrazgo Basin (**MB**) from *Martín-Chivelet et al.* (2019). Columbrets Basin (**CLB**) from *Etheve et al.* (2018) and *Roma et al.* (2018). **VF**: Ventaniella Fault.

Credit author statement

Patricia Cadenas: investigation, conceptualization, methodology, interpretation, validation, writing original draft and review and editing, visualization. **Gianreto Manatschal**: conceptualization, supervision, review and editing, funding acquisition. **Gabriela Fernández-Viejo**: resources, review and editing.

Declaration of Interest Statement

“The authors declare that they have no known competing financial interest or personal relationships that could have appeared to influence the work reported in this paper”.

Research Highlights

1) Multi-stage and overlapped rift systems develop during out of sequence rift events

2) Inherited multi-stage rift templates guide subsequent extension and compression

3) Multi-stage rifting is a keystone on the evolution of divergent plate boundaries

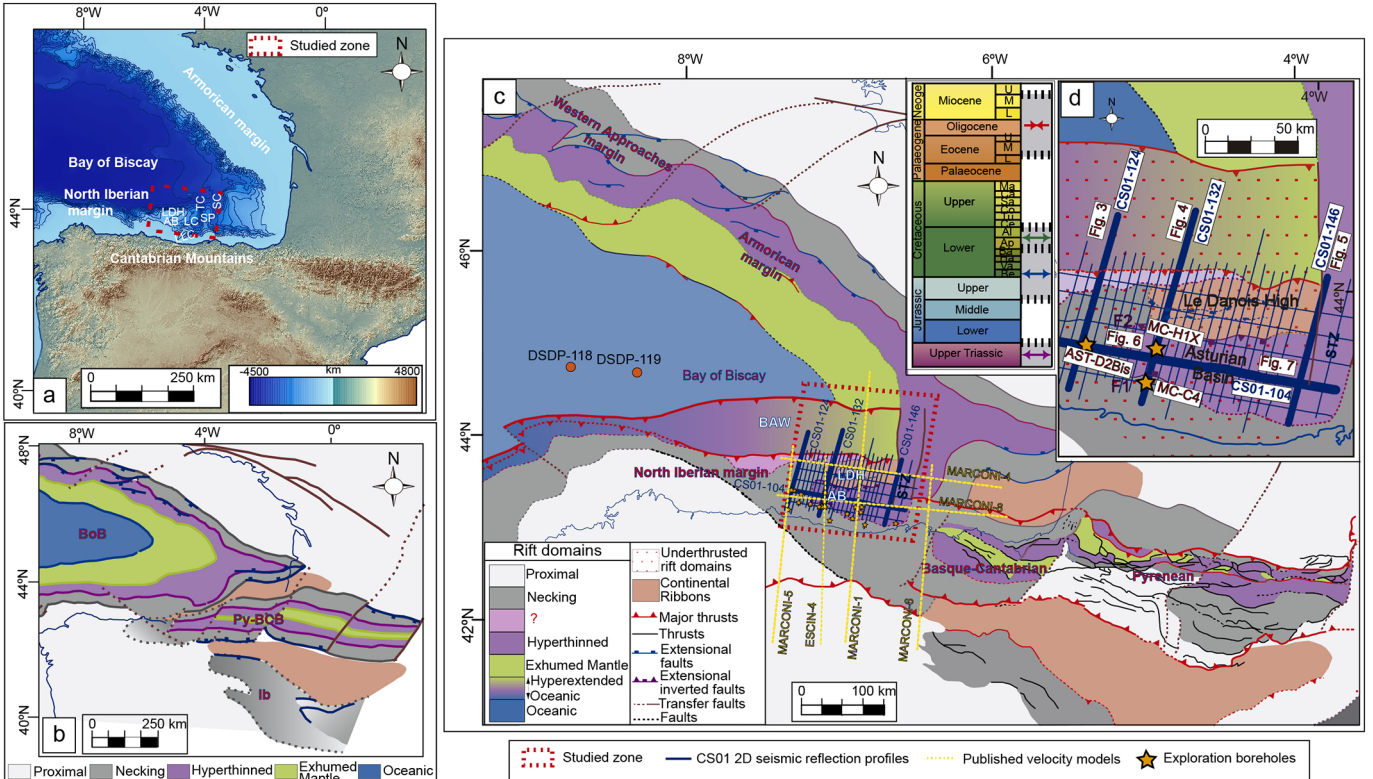
a
Studied zone
Armorican margin
Bay of Biscay
North Iberian margin
LDH
AB
LC
TC
SP
SC
Cantabrian Mountains
8°W
4°W
0°
44°N
40°N
0
250 km
-4500
km
4800
b
BoB
Py-BoB
Ib
48°N
44°N
40°N
Proximal
Necking
Hyperthinned
Exhumed Mantle
Oceanic
c
Western Approaches margin
Armorican margin
DSDP-118
DSDP-119
Bay of Biscay
BAWI
North Iberian margin
CS01-124
CS01-132
CS01-146
CS01-104
MARCONI-4
MARCONI-8
MARCONI-5
ESCIN-4
MARCONI-1
MARCONI-6
Basque-Cantabrian
Pyrenean
6°W
46°N
42°N
Miocene
Oligocene
Eocene
Palaeocene
Upper
Lower
Upper
Middle
Lower
Upper Triassic
Neogene
Palaeogene
Cretaceous
Jurassic
Rift domains
Proximal
Necking
?
Hyperthinned
Exhumed Mantle
Hyperextended
Oceanic
Oceanic
Underthrusted rift domains
Continental Ribbons
Major thrusts
Thrusts
Extensional faults
Extensional inverted faults
Transfer faults
Faults
0
100 km
d
0
50 km
Fig. 3
Fig. 4
Fig. 5
Fig. 6
Fig. 7
Le Danois High
E2
MC-H1X
AST-D2Bis
F1
MC-C4
Asturian Basin
STZ
Studied zone
CS01 2D seismic reflection profiles
Published velocity models
Exploration boreholes

Figure 1

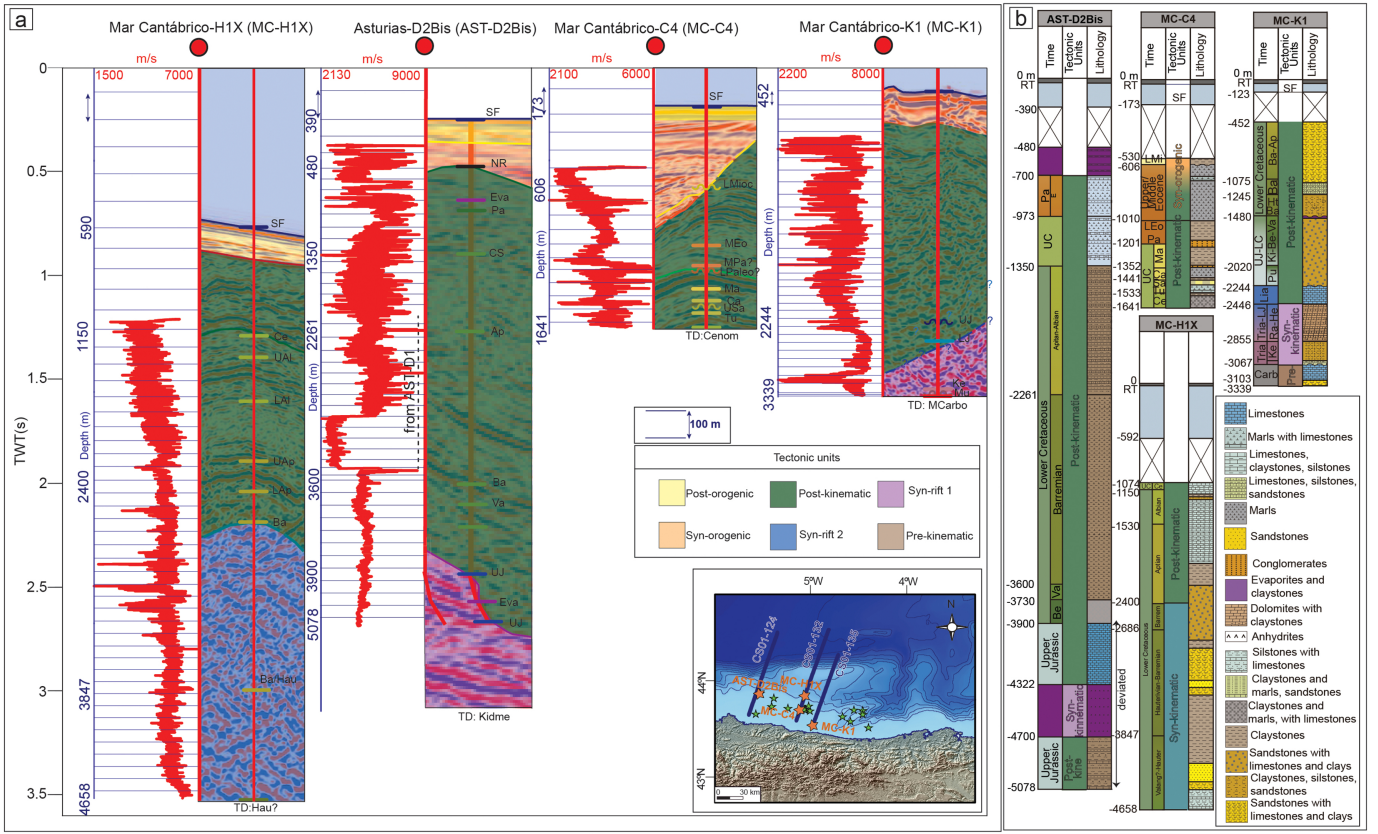
a
Mar Cantábrico-H1X (MC-H1X)
Asturias-D2Bis (AST-D2Bis)
Mar Cantábrico-C4 (MC-C4)
Mar Cantábrico-K1 (MC-K1)
m/s
TWT(s)
Depth (m)
TD:Hau?
TD: Kidme
TD:Cenom
TD: MCarbo
from AST-D1
100 m
Tectonic units
Post-orogenic
Post-kinematic
Syn-rift 1
Syn-orogenic
Syn-rift 2
Pre-kinematic
5ºW
4ºW
44ºN
43ºN
30 km
b
AST-D2Bis
MC-C4
MC-H1X
MC-K1
Time
Tectonic Units
Lithology
deviated
Limestones
Marls with limestones
Limestones, claystones, silstones
Limestones, silstones, sandstones
Marls
Sandstones
Conglomerates
Evaporites and claystones
Dolomites with claystones
Anhydrites
Silstones with limestones
Claystones and marls, sandstones
Claystones and marls, with limestones
Claystones
Sandstones with limestones and clays
Claystones, silstones, sandstones
Sandstones with limestones and clays

Figure 2

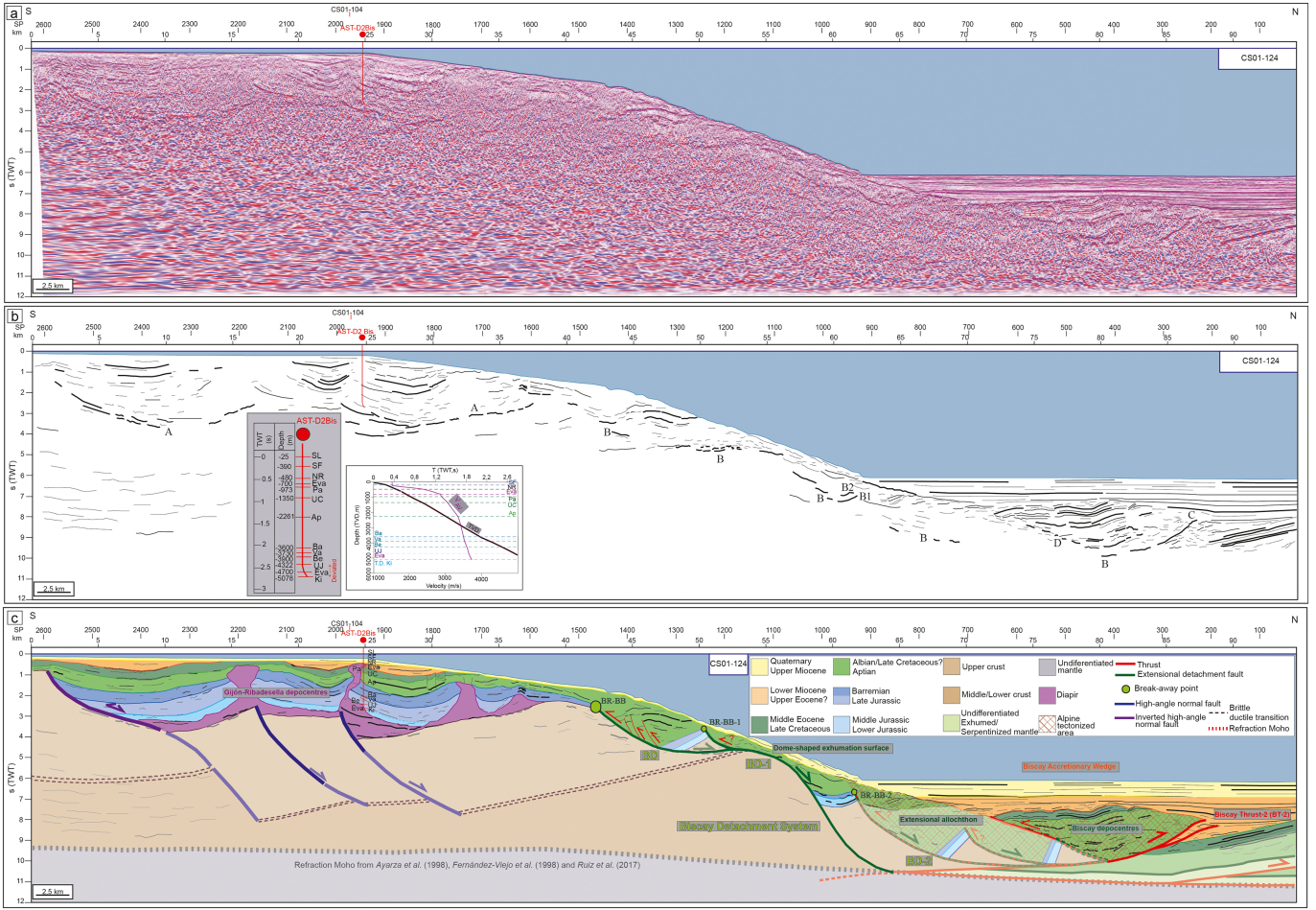
a
b
c
S
N
CS01-104
AST-D2Bis
CS01-124
s (TWT)
2.5 km
SL
SF
NR
Eva
Pa
UC
Ap
Ba
Bs
Br
U
Eva
Kr
Depth (m)
T (TWT,s)
Velocity (m/s)
Depth (TVD, m)
Quaternary
Upper Miocene
Lower Miocene
Upper Eocene?
Middle Eocene
Late Cretaceous
Albian/Late Cretaceous?
Aptian
Barremian
Late Jurassic
Middle Jurassic
Lower Jurassic
Upper crust
Middle/Lower crust
Undifferentiated/
Exhumed/
Serpentinized mantle
Undifferentiated
mantle
Diapir
Alpine
tectonized
area
Thrust
Extensional detachment fault
Break-away point
High-angle normal fault
Inverted high-angle
normal fault
Brittle
ductile transition
Refraction Moho
Gijón-Ribadesella depocentres
BR-BB
BR-BB-1
BR-BB-2
BD
BO-1
BO-2
Dome-shaped exhumation surface
Biscay Accretionary Wedge
Biscay Detachment System
Extensional allochthon
Biscay depocentres
Biscay Thrust-2 (BT-2)
Refraction Moho from Ayarza et al. (1998), Fernández-Viejo et al. (1998) and Ruiz et al. (2017)

Figure 3

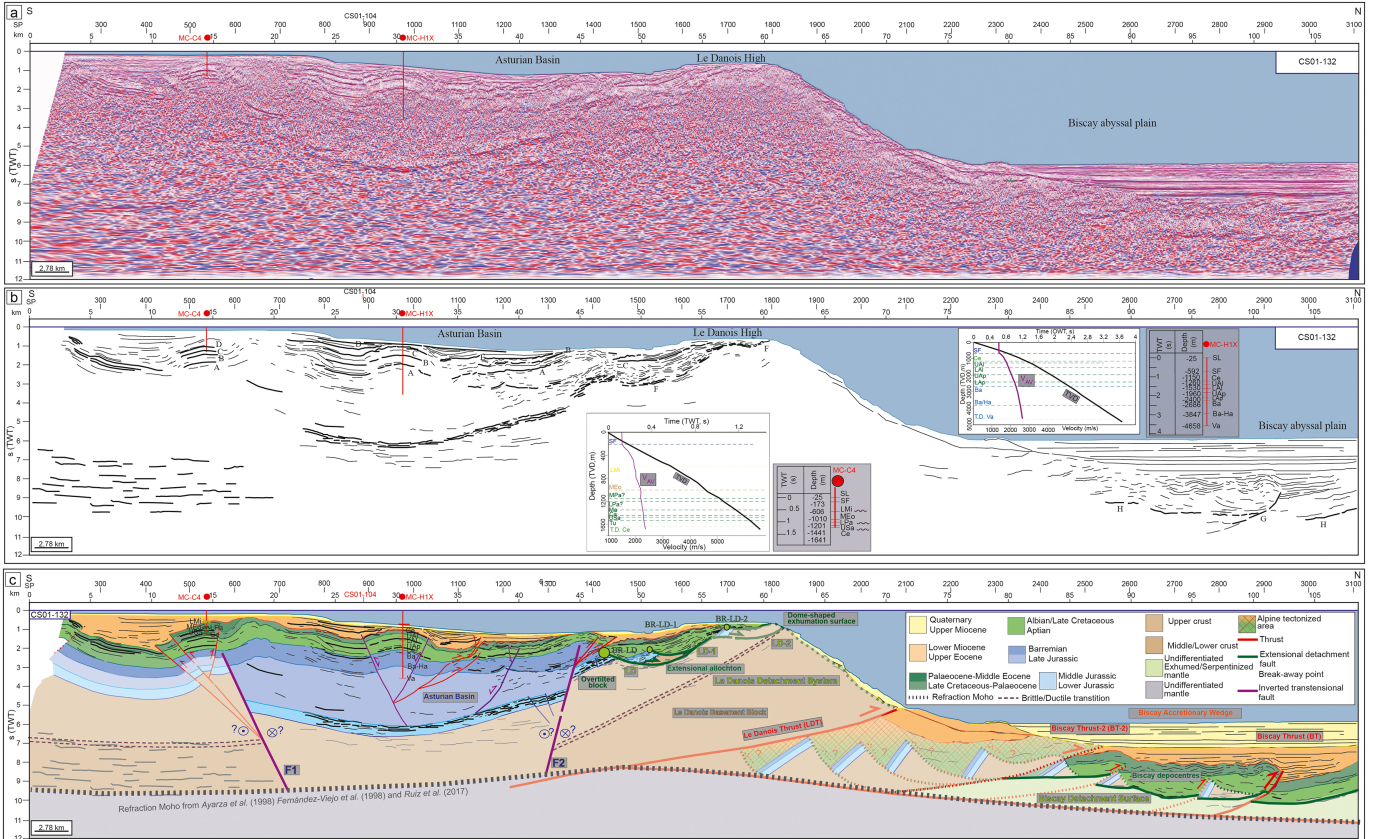
a
b
c
S
N
CS01-104
MC-C4
MC-H1X
CS01-132
Asturian Basin
Le Danois High
Biscay abyssal plain
s (TWT)
2.78 km
Time (TWT, s)
Velocity (m/s)
Depth (TVD m)
TWT (s)
Depth (m)
Le Danois Detachment System
Le Danois Basement Block
Le Danois Thrust (LDT)
Extensional allochton
Overlitted block
Dome-shaped exhumation surface
Biscay Accretionary Wedge
Biscay Thrust-2 (BT-2)
Biscay Thrust (BT)
Biscay Detachment Surface
Biscay depocentres
F1
F2
Refraction Moho from Ayarza et al. (1998) Fernández-Viejo et al. (1998) and Ruiz et al. (2017)
Quaternary
Upper Miocene
Lower Miocene
Upper Eocene
Palaeocene-Middle Eocene
Late Cretaceous-Palaeocene
Albian/Late Cretaceous
Aptian
Barremian
Late Jurassic
Middle Jurassic
Lower Jurassic
Upper crust
Middle/Lower crust
Undifferentiated Exhumed/Serpentinized mantle
Undifferentiated mantle
Refraction Moho
Brittle/Ductile transition
Alpine tectonized area
Thrust
Extensional detachment fault
Break-away point
Inverted transtensional fault

Figure 4

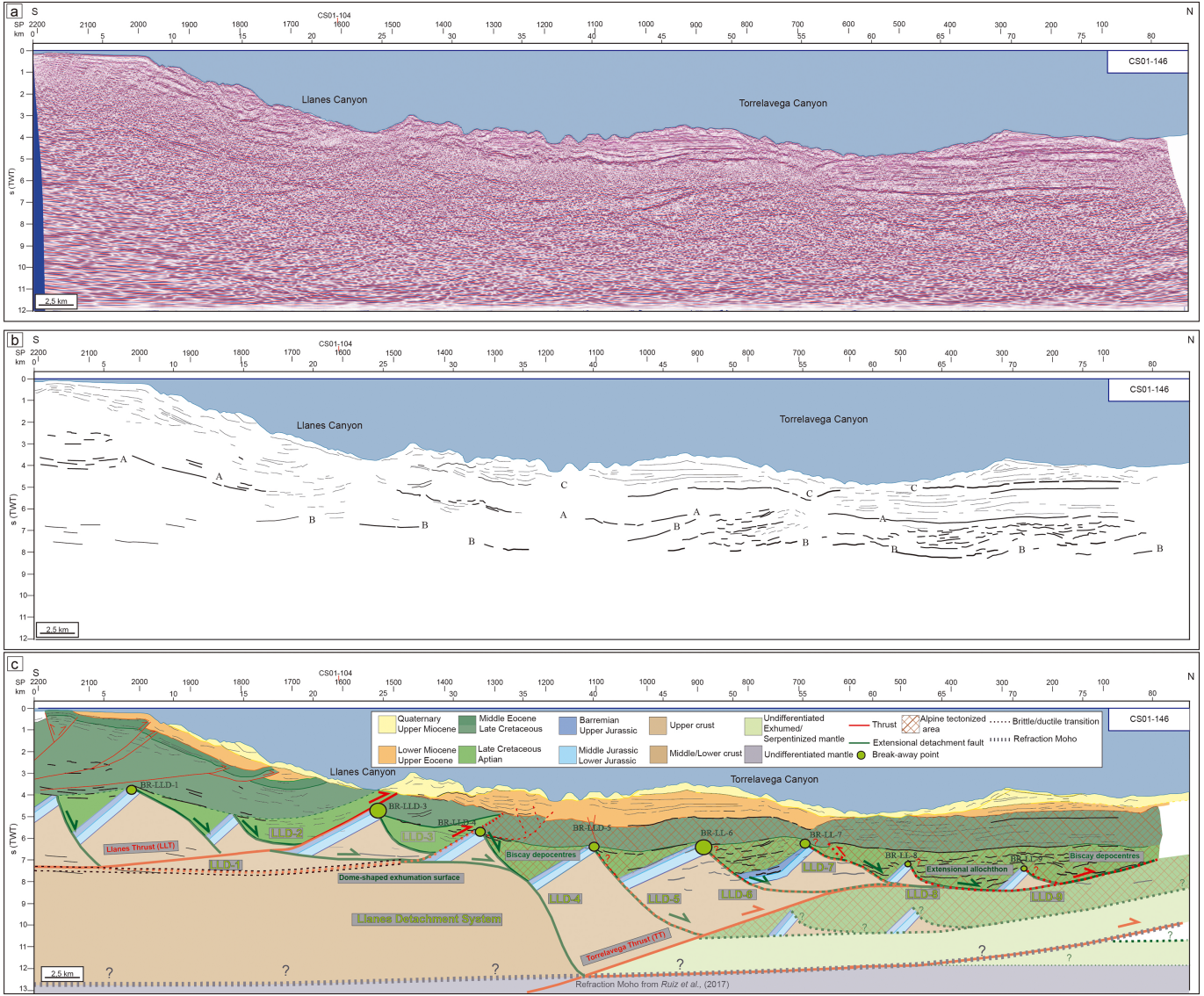
a
b
c
S
N
CS01-104
CS01-146
SP
km
s (TWT)
Llanes Canyon
Torrelavega Canyon
2.5 km
Quaternary
Upper Miocene
Middle Eocene
Late Cretaceous
Barremian
Upper Jurassic
Upper crust
Undifferentiated
Exhumed/
Serpentinized mantle
Thrust
Alpine tectonized
area
Brittle/ductile transition
Lower Miocene
Upper Eocene
Late Cretaceous
Aptian
Middle Jurassic
Lower Jurassic
Middle/Lower crust
Undifferentiated mantle
Extensional detachment fault
Break-away point
Refraction Moho
BR-LLD-1
BR-LLD-3
BR-LLD-4
BR-LLD-5
BR-LL-6
BR-LL-7
BR-LL-8
BR-LL-9
LLD-2
LLD-3
LLD-4
LLD-5
LLD-6
LLD-7
LLD-8
LLD-9
Llanes Thrust (LLT)
Biscay depocentres
Dome-shaped exhumation surface
Extensional allochthon
Llanes Detachment System
Torrelavega Thrust (TT)
Refraction Moho from Ruiz et al., (2017)

Figure 5

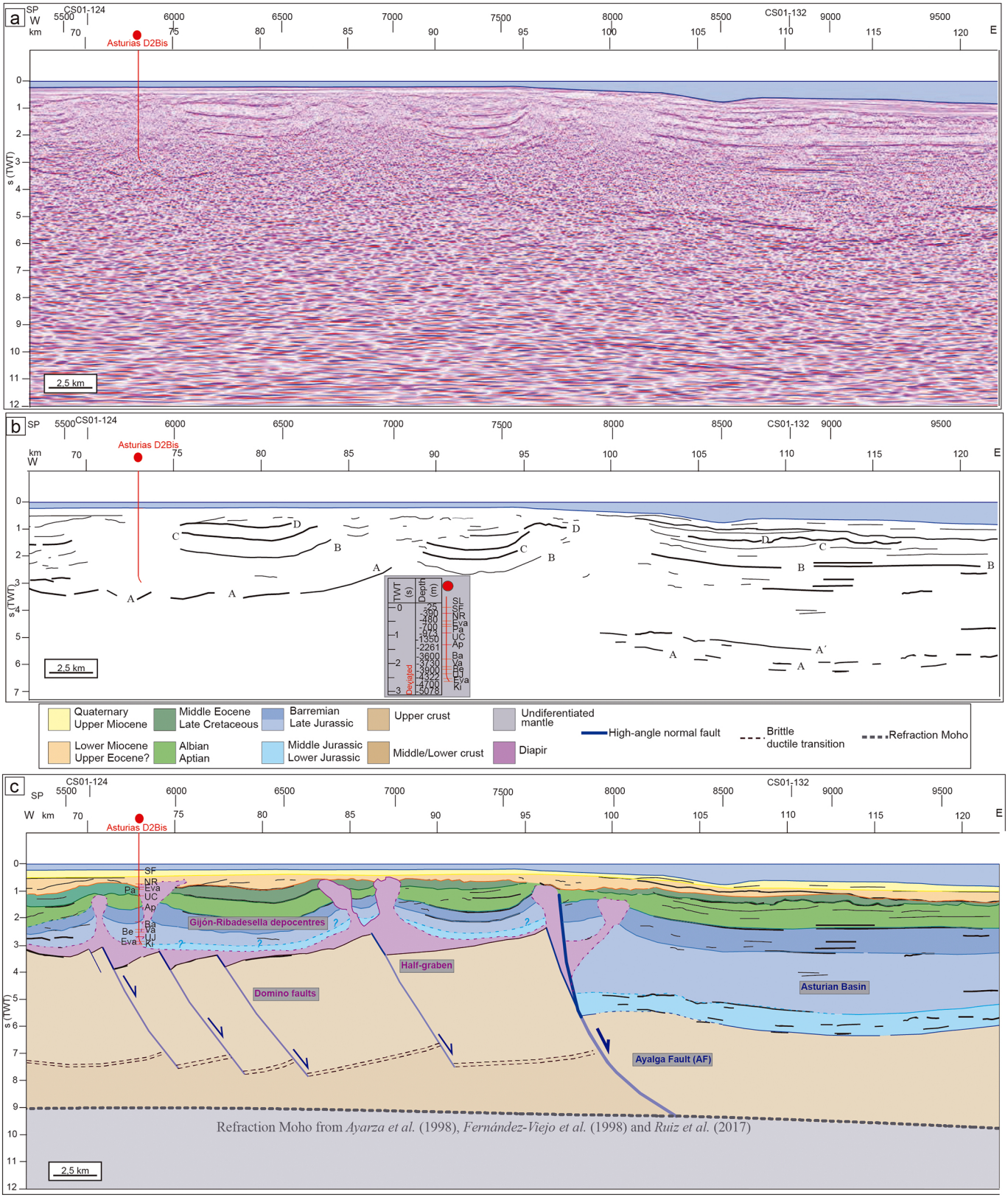
a
b
c
SP
W
km
E
CS01-124
CS01-132
Asturias D2Bis
s (TWT)
2,5 km
TWT (s)
Depth (m)
Deviated
SL
SO
NR
Eva
Pa
UC
Ap
Ba
Va
UJ
Be
Eva
Ki
A
A'
B
C
D
Quaternary
Upper Miocene
Lower Miocene
Upper Eocene?
Middle Eocene
Late Cretaceous
Albian
Aptian
Barremian
Late Jurassic
Middle Jurassic
Lower Jurassic
Upper crust
Middle/Lower crust
Undiferentiated
mantle
Diapir
High-angle normal fault
Brittle
ductile transition
Refraction Moho
Gijón-Ribadesella depocentres
Half-graben
Domino faults
Asturian Basin
Ayalga Fault (AF)
Refraction Moho from Ayarza et al. (1998), Fernández-Viejo et al. (1998) and Ruiz et al. (2017)

Figure 6

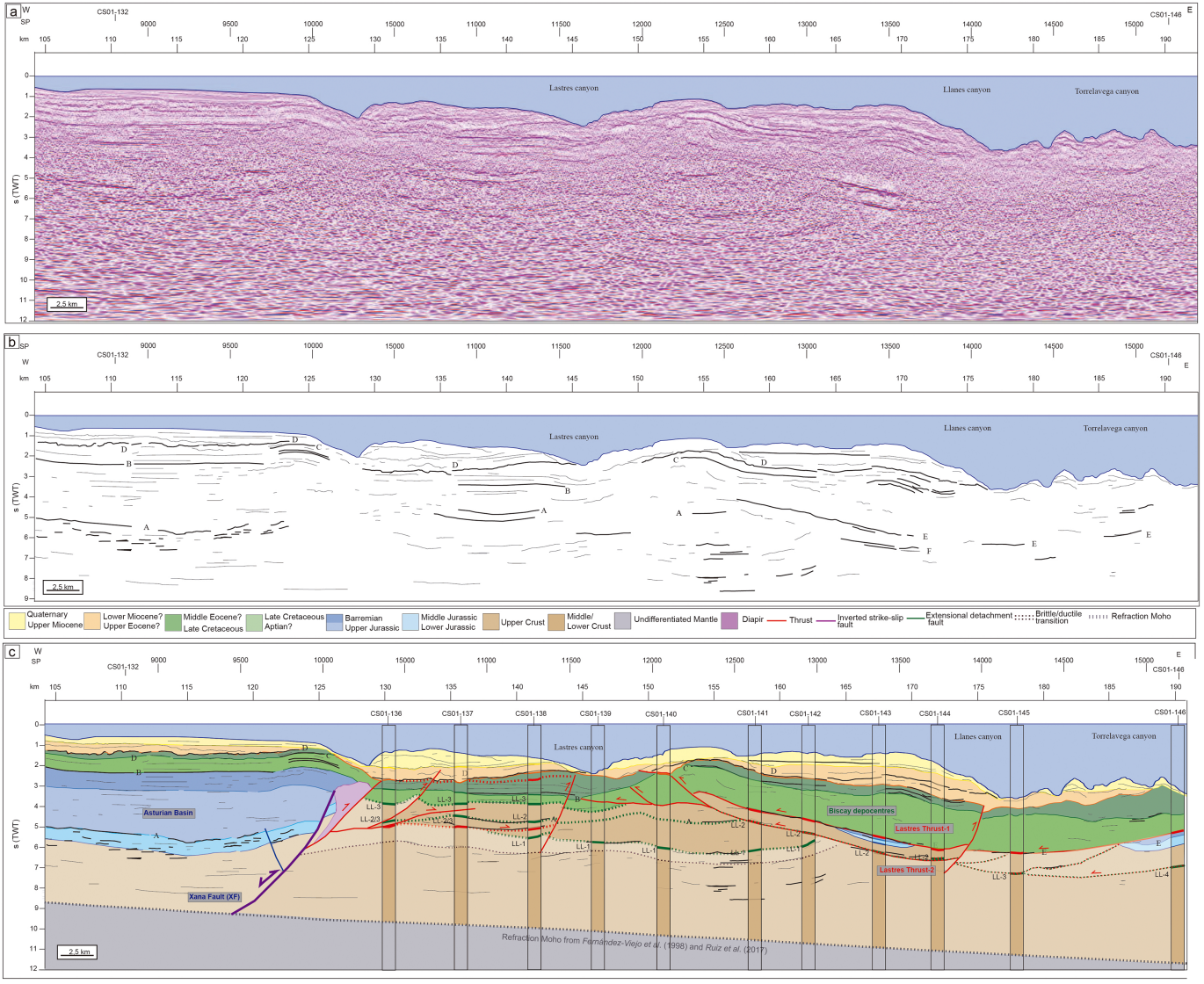
a
W
E
SP
CS01-132
CS01-146
km
s (TWT)
Lastres canyon
Llanes canyon
Torrelavega canyon
2.5 km
b
Lastres canyon
Llanes canyon
Torrelavega canyon
2.5 km
Quaternary
Upper Miocene
Lower Miocene?
Upper Eocene?
Middle Eocene?
Late Cretaceous
Late Cretaceous
Aptian?
Barremian
Upper Jurassic
Middle Jurassic
Lower Jurassic
Upper Crust
Middle/
Lower Crust
Undifferentiated Mantle
Diapir
Thrust
Inverted strike-slip fault
Extensional detachment fault
Brittle/ductile transition
Refraction Moho
c
CS01-136
CS01-137
CS01-138
CS01-139
CS01-140
CS01-141
CS01-142
CS01-143
CS01-144
CS01-145
Asturian Basin
Xana Fault (XF)
Biscay depocentres
Lastres Thrust-1
Lastres Thrust-2
Refraction Moho from Fernández-Viejo et al. (1998) and Ruiz et al. (2017)
2.5 km

Figure 7

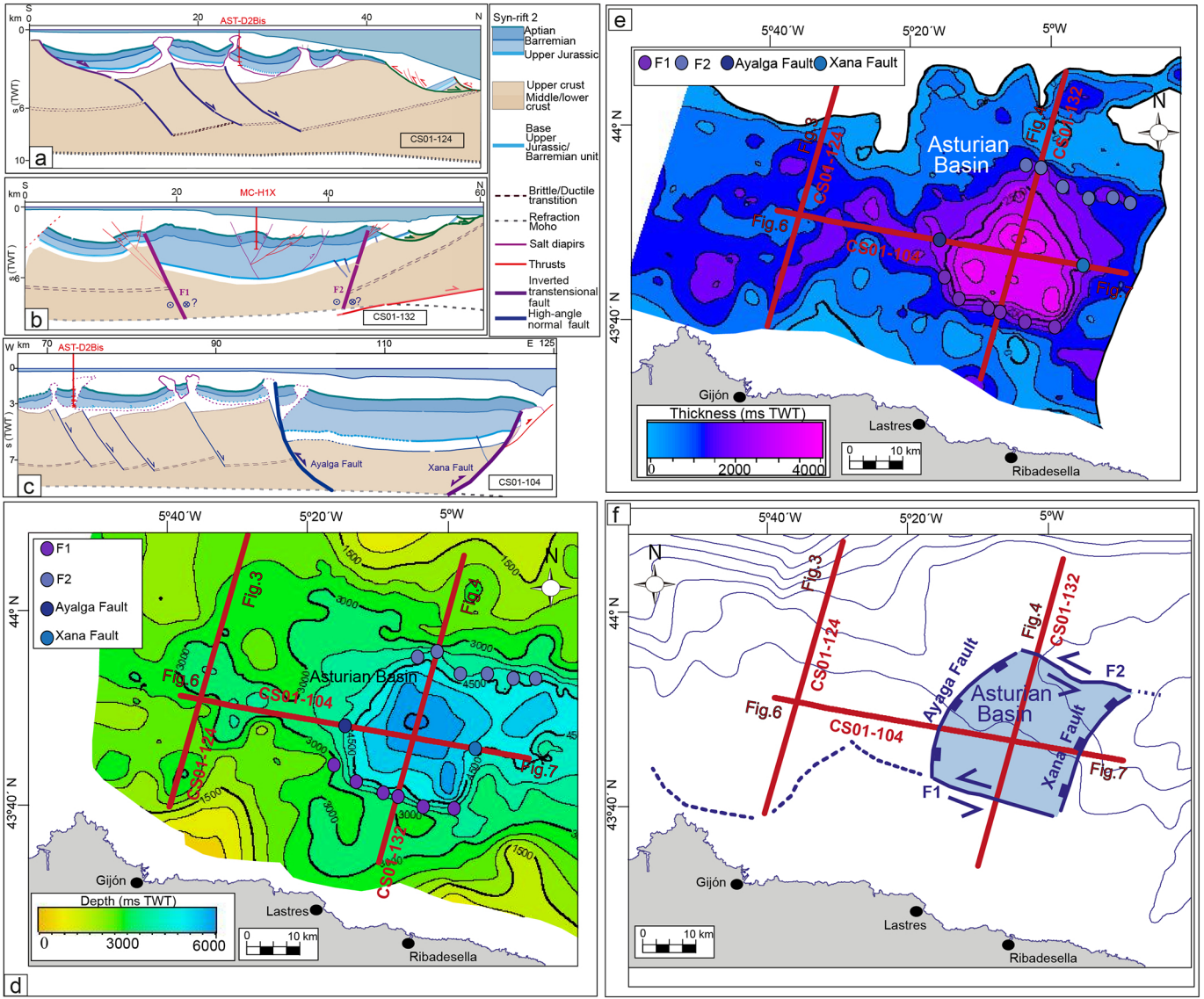
a
AST-D2Bis
CS01-124
b
MC-H1X
F1
F2
CS01-132
c
AST-D2Bis
Ayalga Fault
Xana Fault
CS01-104
Syn-rift 2
Aptian
Barremian
Upper Jurassic
Upper crust
Middle/lower crust
Base Upper Jurassic/ Barremian unit
Brittle/Ductile transition
Refraction Moho
Salt diapirs
Thrusts
Inverted transtensional fault
High-angle normal fault
d
F1
F2
Ayalga Fault
Xana Fault
Asturian Basin
Fig.3
Fig.4
Fig.6
Fig.7
CS01-104
CS01-124
CS01-132
Depth (ms TWT)
Gijón
Lastres
Ribadesella
e
F1
F2
Ayalga Fault
Xana Fault
Asturian Basin
Thickness (ms TWT)
f
Asturian Basin
Ayalga Fault
Xana Fault
F1
F2

Figure 8

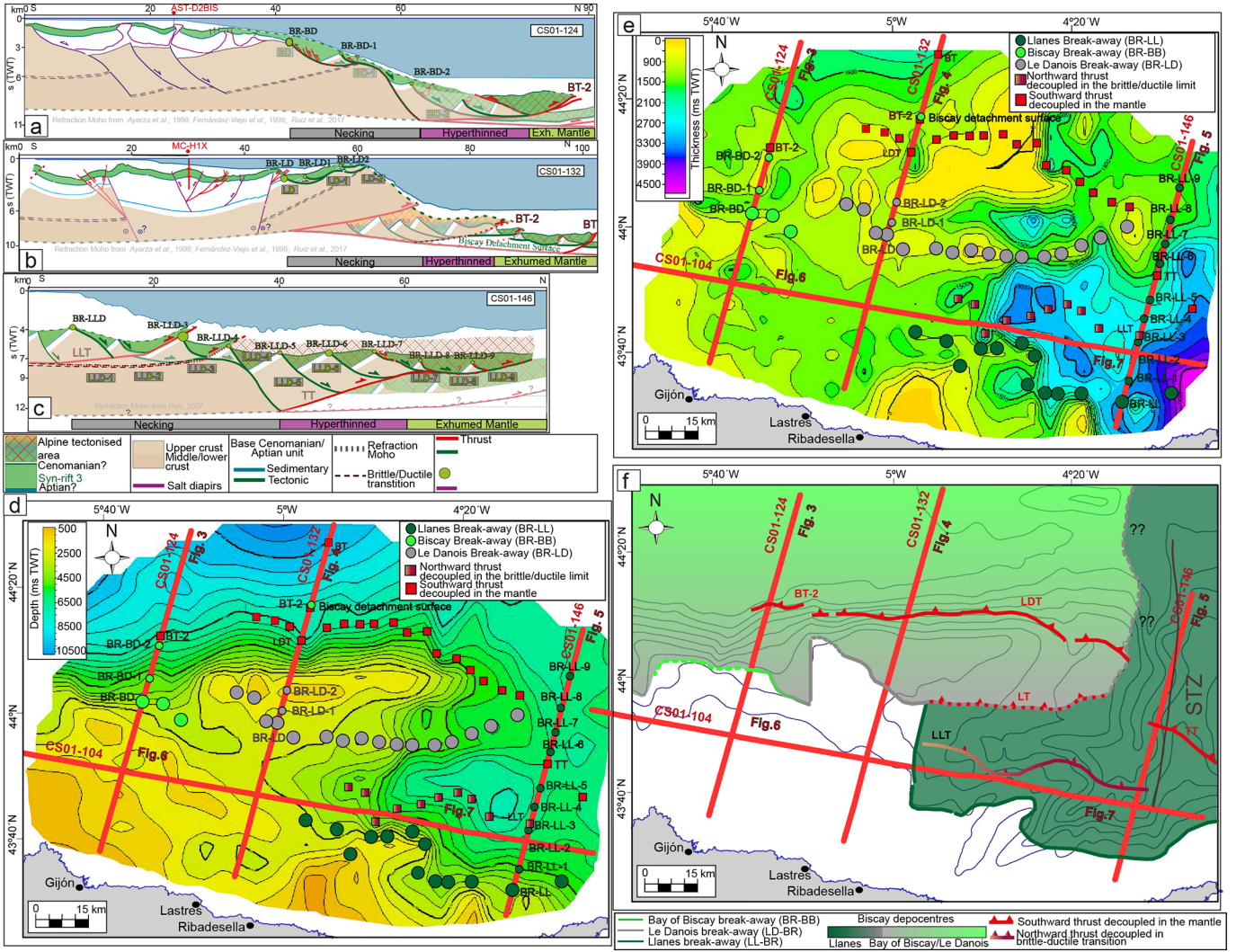
AST-D2BIS
CS01-124
BR-BD
BR-BD-1
BR-BD-2
BT-2
BT
Refraction Moho from Ayarza et al., 1998; Fernández-Viejo et al., 1998; Ruiz et al., 2017
Necking
Hyperthinned
Exh. Mantle
a
MC-H1X
CS01-132
BR-LD
BR-LD1
BR-LD2
Biscay Detachment Surface
Exhumed Mantle
b
CS01-146
BR-LLD
BR-LLD-3
BR-LLD-4
BR-LLD-5
BR-LLD-6
BR-LLD-7
BR-LLD-8
BR-LLD-9
LLT
TT
Refracting Moho from Ruiz, 2007
c
Alpine tectonised area
Cenomanian?
Syn-rift 3
Aptian?
Upper crust
Middle/lower crust
Salt diapirs
Base Cenomanian/ Aptian unit
Sedimentary
Tectonic
Refraction Moho
Brittle/Ductile transition
Thrust
d
5°40´W
5°W
4°20´W
44°20´N
44°N
43°40´N
Depth (ms TWT)
Llanes Break-away (BR-LL)
Biscay Break-away (BR-BB)
Le Danois Break-away (BR-LD)
Northward thrust decoupled in the brittle/ductile limit
Southward thrust decoupled in the mantle
Biscay detachment surface
CS01-104
Fig.6
Fig.7
Gijón
Lastres
Ribadesella
0 15 km
e
Thickness (ms TWT)
f
STZ
??
Bay of Biscay break-away (BR-BB)
Le Danois break-away (LD-BR)
Llanes break-away (LL-BR)
Biscay depocentres
Llanes
Bay of Biscay/Le Danois
Southward thrust decoupled in the mantle
Northward thrust decoupled in brittle-ductile transition

Figure 9

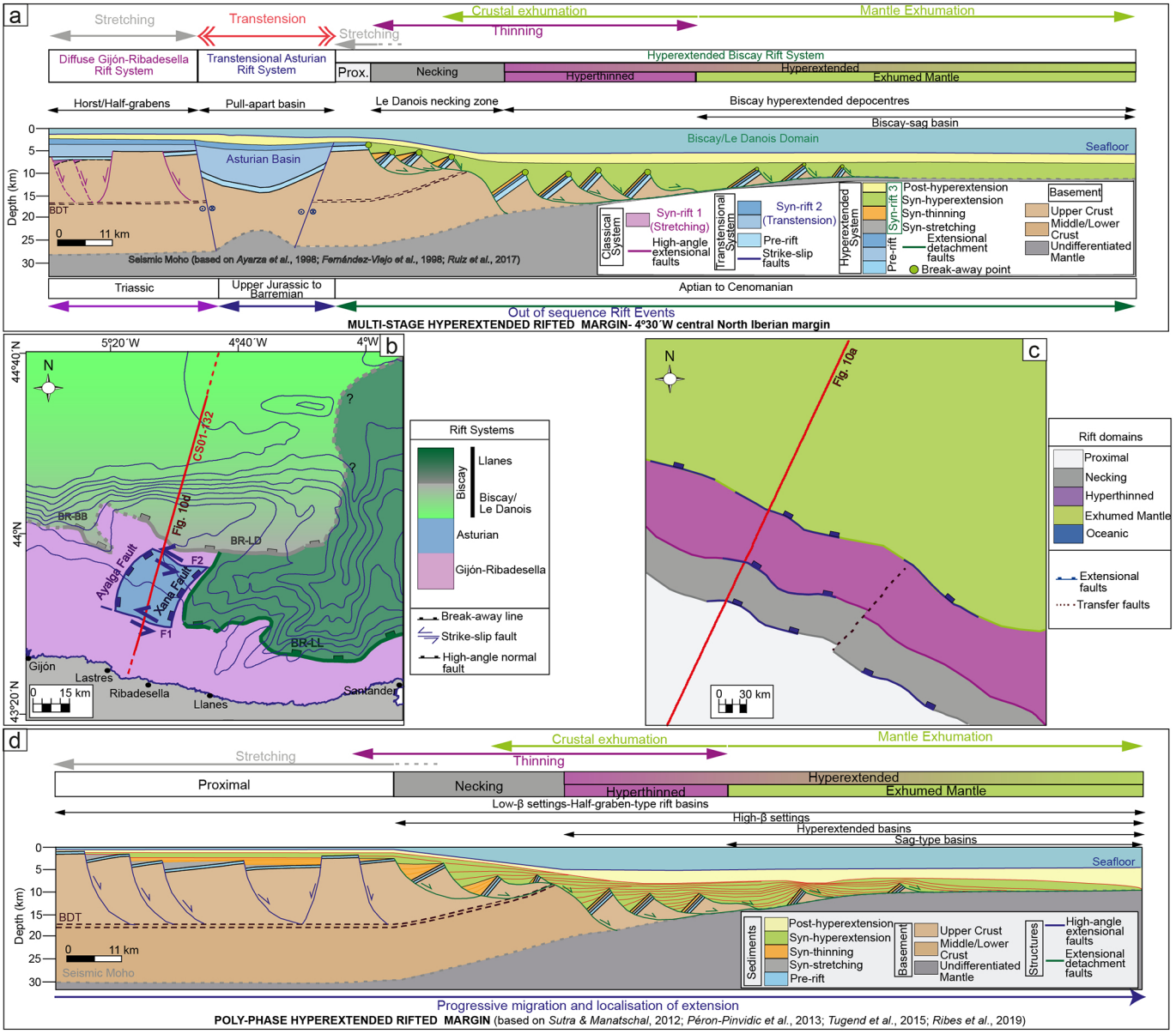
a
Stretching
Transtension
Stretching
Crustal exhumation
Thinning
Mantle Exhumation
Diffuse Gijón-Ribadesella Rift System
Transtensional Asturian Rift System
Hyperextended Biscay Rift System
Prox.
Necking
Hyperthinned
Hyperextended
Exhumed Mantle
Horst/Half-grabens
Pull-apart basin
Le Danois necking zone
Biscay hyperextended depocentres
Biscay-sag basin
Biscay/Le Danois Domain
Seafloor
Asturian Basin
BDT
0 11 km
Depth (km)
Seismic Moho (based on Ayarza et al., 1998; Fernández-Viejo et al., 1998; Ruiz et al., 2017)
Classical System
Syn-rift 1 (Stretching)
High-angle extensional faults
Transtensional System
Syn-rift 2 (Transtension)
Pre-rift
Strike-slip faults
Hyperextended System
Syn-rift 3
Pre-rift
Post-hyperextension
Syn-hyperextension
Syn-thinning
Syn-stretching
Extensional detachment faults
Break-away point
Basement
Upper Crust
Middle/Lower Crust
Undifferentiated Mantle
Triassic
Upper Jurassic to Barremian
Aptian to Cenomanian
Out of sequence Rift Events
MULTI-STAGE HYPEREXTENDED RIFTED MARGIN- 4°30´W central North Iberian margin
b
5°20´W
4°40´W
4°W
44°40´N
44°N
43°20´N
N
CS01-132
Fig. 10d
BR-BB
BR-LD
BR-LL
Ayaga Fault
Xana Fault
F1
F2
Gijón
Lastres
Ribadesella
Llanes
Santander
0 15 km
Rift Systems
Biscay
Llanes
Biscay/ Le Danois
Asturian
Gijón-Ribadesella
Break-away line
Strike-slip fault
High-angle normal fault
c
N
Fig. 10a
0 30 km
Rift domains
Proximal
Necking
Hyperthinned
Exhumed Mantle
Oceanic
Extensional faults
Transfer faults
d
Stretching
Crustal exhumation
Thinning
Mantle Exhumation
Proximal
Necking
Hyperextended
Hyperthinned
Exhumed Mantle
Low-β settings-Half-graben-type rift basins
High-β settings
Hyperextended basins
Sag-type basins
Seafloor
BDT
0 11 km
Seismic Moho
Depth (km)
Sediments
Post-hyperextension
Syn-hyperextension
Syn-thinning
Syn-stretching
Pre-rift
Basement
Upper Crust
Middle/Lower Crust
Undifferentiated Mantle
Structures
High-angle extensional faults
Extensional detachment faults
Progressive migration and localisation of extension
POLY-PHASE HYPEREXTENDED RIFTED MARGIN (based on Sutra & Manatschal, 2012; Péron-Pinvidic et al., 2013; Tugend et al., 2015; Ribes et al., 2019)

Figure 10

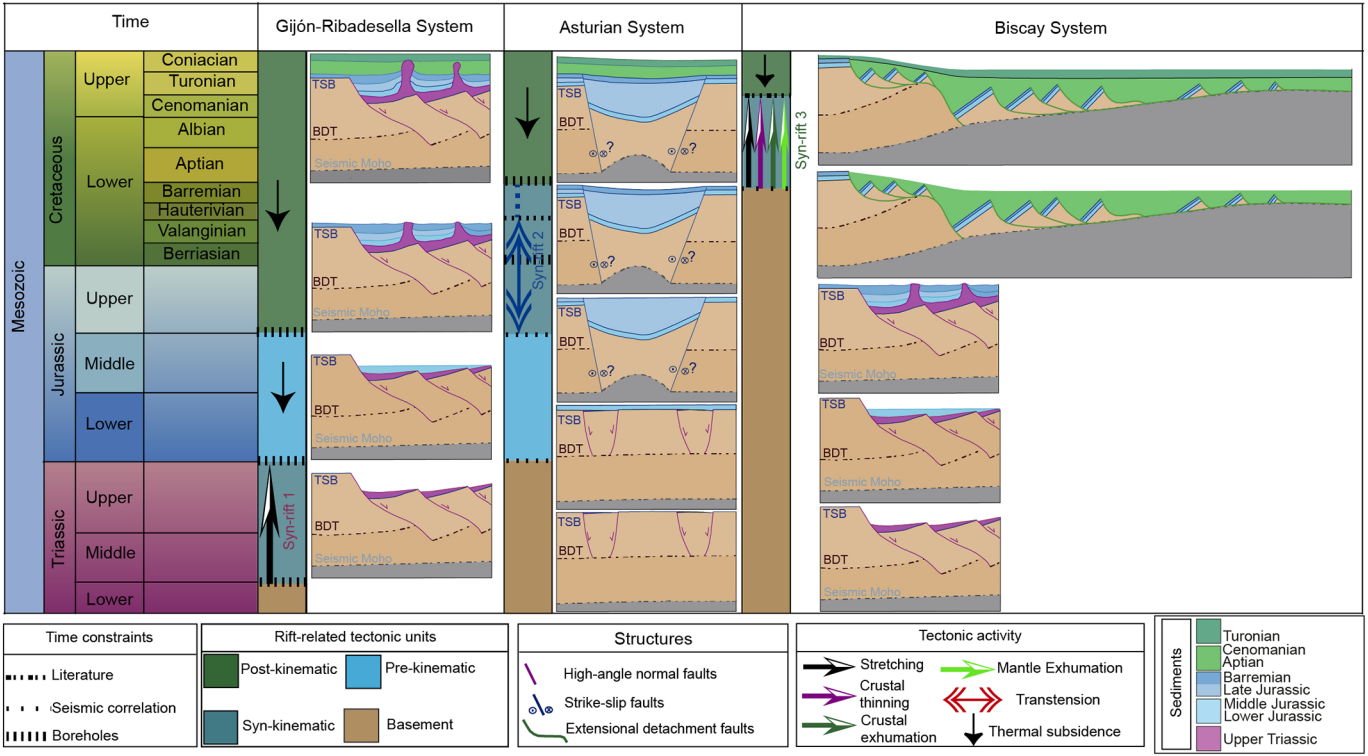
Time
Gijón-Ribadesella System
Asturian System
Biscay System
Mesozoic
Cretaceous
Upper
Lower
Coniacian
Turonian
Cenomanian
Albian
Aptian
Barremian
Hauterivian
Valanginian
Berriasian
Jurassic
Upper
Middle
Lower
Triassic
Upper
Middle
Lower
TSB
BDT
Seismic Moho
Syn-rift 1
Syn-rift 2
Syn-rift 3
Time constraints
Literature
Seismic correlation
Boreholes
Rift-related tectonic units
Post-kinematic
Pre-kinematic
Syn-kinematic
Basement
Structures
High-angle normal faults
Strike-slip faults
Extensional detachment faults
Tectonic activity
Stretching
Crustal thinning
Crustal exhumation
Mantle Exhumation
Transtension
Thermal subsidence
Sediments
Turonian
Cenomanian
Aptian
Barremian
Late Jurassic
Middle Jurassic
Lower Jurassic
Upper Triassic

Figure 11

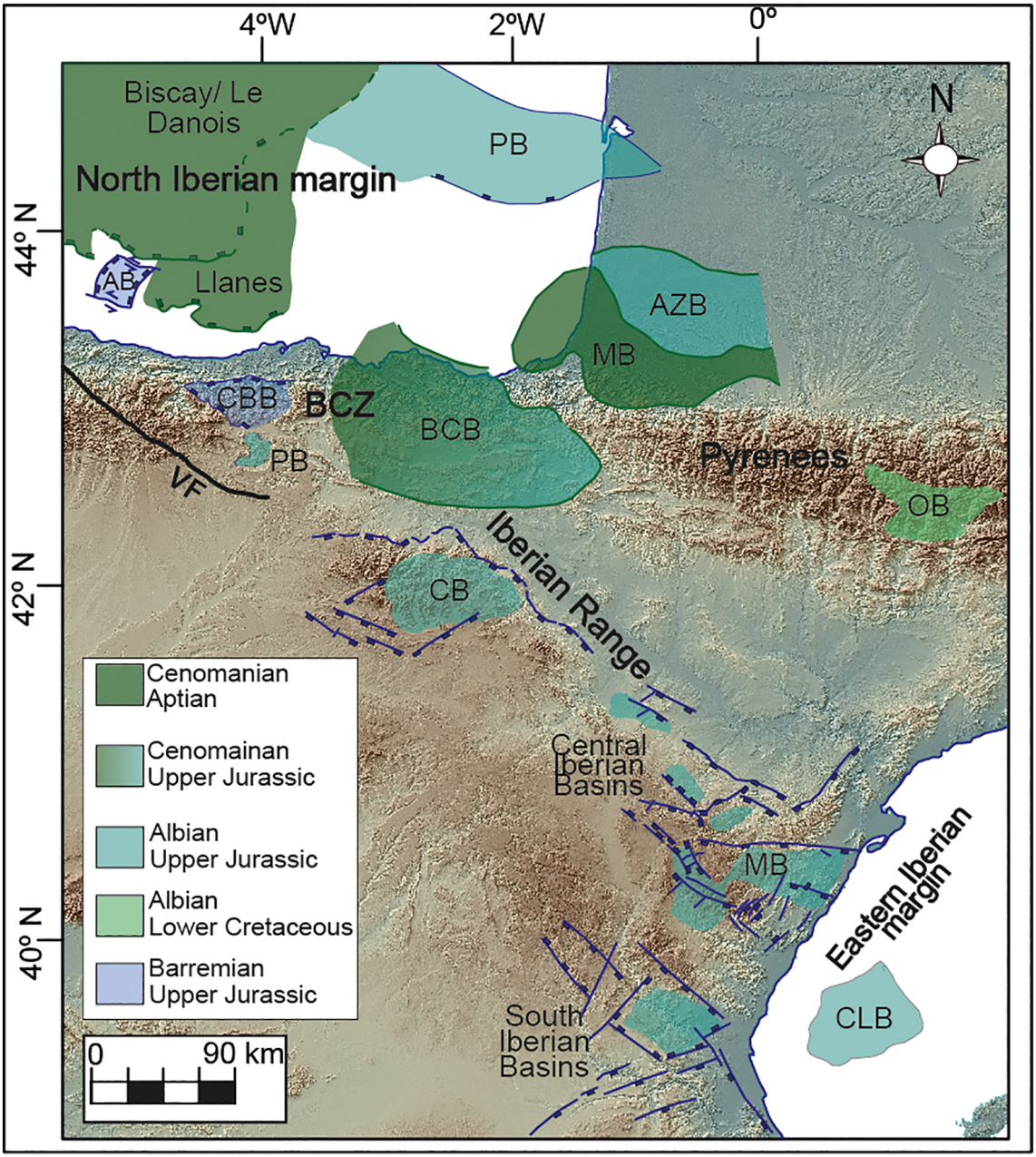
4°W
2°W
0°
44° N
42° N
40° N
N
Biscay/ Le Danois
North Iberian margin
PB
AB
Llanes
AZB
MB
CBB
BCZ
BCB
PB
VF
Pyrenees
OB
CB
Iberian Range
Central Iberian Basins
MB
Eastern Iberian margin
CLB
South Iberian Basins
Cenomanian Aptian
Cenomainan Upper Jurassic
Albian Upper Jurassic
Albian Lower Cretaceous
Barremian Upper Jurassic
0
90 km

Figure 12